Porous Janus materials with unique asymmetries and functionality

Linlin Yan†[a], Xiaobin Yang†[a,b], Yanqiu Zhang[a,c], Yadong Wu[a], Zhongjun Cheng[a], Seth B. Darling*[b], Lu Shao*[a]

a Chemical Engineering, Harbin Institute of Technology, Harbin 150001, P. R. China

[b] Advanced Materials for Energy-Water Systems (AMEWS) Energy Frontier Research Center, Center for Molecular Engineering, and Chemical Sciences and Engineering Division, Argonne National Laboratory, Lemont, IL 60439, USA

[c] School of Environments, Harbin Institute of Technology, Harbin 150009, China.

† These authors contributed equally to this work.

***Corresponding Author:**

Email address:

darling@anl.gov (Seth B. Darling)

shaolu@hit.edu.cn (L. Shao)

Contents

1. Introduction

2. Fabrications of porous Janus materials

2.1. Direct/sequential assembly into Janus materials

2.2. In situ generation of Janus materials

2.3. Asymmetric modification into Janus materials

2.3.1. Phase boundary strategies

2.3.2 Non-boundary strategies

2.4. Multifunction integration into Janus materials

3. Work mechanisms of porous Janus materials

3.1 Synergistic mode of asymmetry

3.1.1 Directional liquid transport

3.1.2 Directional bubble transport

3.1.3 Rectified ion transport

3.2 Independent mode of asymmetry

4. Summary and Outlook

Abstract

Porous Janus materials have attracted widespread attention due to their asymmetry in wettability, charge, pore size or structure, thermal/electrical conductivity, and chemical activity. Multifunction integration and unique directional manipulation of liquid, ion, or gas within porous Janus materials enable rapid progress in diverse applications such as fog collection, personal moisture and healthcare management, energy conversion, water purification, sensor devices, and biomedical applications. Compared with conventional homogeneous materials, porous Janus materials not only showcase superior performance and energetic potential but also open up new applications by virtue of the synergistic or independent effects of asymmetry. This comprehensive review systematically analyzes the research progress of porous Janus materials, highlighting fabrication strategies, synergistic/independent work mechanisms, and emerging advanced applications. Finally, ongoing challenges and outlook for the future research of porous Janus materials are presented.

Keywords: porous materials, Janus materials, asymmetry, directional transport, multifunction integration

1 Introduction

Ever-increasing diversified and complex materials-based demands necessitate exploitation of novel materials with multifunction integration or advanced functionality[1-5]. Therein, artificial Janus materials (natural Janus materials are ubiquitous such as cell membranes for ionic transport[6]), named after the two-faced god Janus in ancient Roman mythology, have two faces with asymmetric properties and came to light after P. G. de Gennes' Nobel Prize lecture in 1991[7]. Originally, efforts were focused on fabricating materials on the micro-/nano-scale, such as Janus particles/nanosheets/cylinders with two different compositions, morphologies, or sizes, finding applications as solid emulsion stabilizers, optical probes, and catalysts[8,9]. Afterward, this sector expanded Janus materials to the macroscopic scale, and Lin et al.[10] realized directional water-transfer by asymmetric wettability integration across material thickness, which cannot be accomplished by conventional homogeneous porous materials. To date, the exploited asymmetric properties of porous Janus materials at the macroscopic level include wettability, charge, pore size/structure, thermal/electrical conductivity, and chemical activity, but are not limited to these.

There are two working modes for asymmetric properties of porous Janus materials: synergistic and independent. In the synergistic mode, porous Janus materials will present unique diode performance. For asymmetric wettability such as hydrophobic/hydrophilic[11] and super-oleophobic/super-oleophilic[12], these porous Janus materials can realize directional liquid transport such as water/oil "diodes"[13,14] (liquid penetrating from one side and being blocked in the reverse direction) when regulating appropriate wettability, pore size, and thickness of the functional layers, which promises applications in advanced separation[15], fog collection[16], healthcare[17], moisture

absorption and perspiration[18]. Hydrophobic/hydrophilic Janus porous materials are also aerophilic/aerophobic in water, enabling realization of bubble unidirectional transport underwater (air ‘‘diode’’)[19,20] and applications of water-splitting[21] or superior gas transport[22]. Distinguished from conventional homogeneous materials, asymmetric wettability provides an inner driving force for facilitating liquid or bubble transport, which improves operational energy efficiency[23,24]. In addition, architectures with charge asymmetry enable porous Janus materials as ion diodes, which can capture osmotic energy from natural systems[25]. In the independent mode, porous Janus materials tend to be multifunctional and integrated, which showcase superior performance or open up new application fields. The asymmetric properties work separately without interfering with each other, which can realize the coexistence of various functionalities for a variety of applications in water purification, sensors, and in the biomedical field. For example, hydrophilic/hydrophobic Janus membranes can deliver functionality of both hydrophilic and hydrophobic membranes to separate or generate different emulsions[26,27]. Integrating asymmetric properties can also decouple application processes to achieve superior performance. As an example, solar desalination can be broken down into water pumping by the hydrophilic layer and light-heat conversion and steam generation by the hydrophobic layer. The presence of the hydrophilic layer mitigates salt deposition, which has been an important obstacle to efficiency for conventional materials[28].

Other investigations have explored the combination of Janus character with other emerging functional materials such as graphene oxide (GO)[29], MXene[30], carbon nanotubes (CNTs)[31], or stimulation-responsive substances[13,32,33], which greatly enriches the function and application space of porous Janus materials. In addition, porous Janus materials can also possess two or more asymmetric properties in one unit

at the same time, which results in tremendous variety and opportunities for multi-application[34-36]. These achievements demonstrate that porous Janus materials present enormous potential in constructing advanced and intelligent devices.

This review aims to provide a concise and comprehensive overview (Fig. 1), systematically summarizing recent advances in various asymmetry and fabrication strategies, highlighting the two working mechanisms of asymmetry of porous Janus materials, discussing their multi-functional application in water-oil separation, fog collection, personal moisture and healthcare management, energy conversion, desalination, sensor devices, and biomedical applications in detail, and finally, offering the challenges and outlook for future development of porous macroscopic Janus materials.

2 Fabrications of porous Janus materials

Porous Janus materials, featured by asymmetric properties on two opposing surfaces, can be organic, inorganic, or hybrid/composite[37]. In comparison with microscopic Janus particles[38] and nanosheets[39], the porous Janus materials that we review here are macroscopic and promise wider applications. To date, a variety of asymmetric properties have been exploited, which can be independent bi-/tri-layer, gradient, or interpenetrating along the material thickness, including wettability, charge, pore size or structure, thermal or electrical conductivity, and chemical activity. In general, porous Janus materials can be prepared by direct/sequential assembly, in situ generation, and asymmetric modification according to the requirements in practice, which is shown in detail in Table 1. Beyond those aforementioned isolated Janus materials, emerging multifunctional porous Janus materials have been gaining attention via multifunction

integration during materials fabrication due to their broader library of performance features.

2.1 Direct/sequential assembly into Janus materials

The most straightforward route is a direct combination of two materials, such as integration of a hydrophobic copper mesh and a super-hydrophilic cotton absorbent on a water column as a Janus system (Fig. 2a)[16,40]. However, the properties or functionalities of the obtained Janus materials may be limited by the inherent properties of the original materials. Therefore, in order to achieve controlled fabrication of Janus materials, many researchers have focused on preparing the two layers sequentially to construct asymmetry for porous Janus materials. Electrospinning technology is promising to generate various nanofibers for widespread applications[41], due to the diversity of the spinning solution, such as hydrophilic poly (vinyl alcohol)[42], polyacrylonitrile (PAN)[43,44], polylactic acid[45], or hydrophobic polyurethane (PU)[46], and polyvinylidene fluoride (PVDF)[47,48]. The deposited layer's thickness, pore size, roughness, and chemical properties can be systematically controlled by tuning operation time, solute concentration, chemical components, or additives[49-53]. For example, electrospinning can prepare two layers in sequence with different pore size by adjusting fiber diameter and stacking thickness to construct Janus materials (Fig. 2b)[54,55]. In general, a higher concentration of the spinning solution and a larger inner diameter of the nozzle can form coarser filaments and bigger apertures. Electrodeposition technology is also an effective method to deposit polymer layers due to the migration of charged polymers under an electric field. As shown in Fig. 2c, the different conformations of the polycation amino-polysaccharide chitosan were utilized in the absence or presence of soluble NaH_2PO_4 to prepare Janus films with asymmetric

pore sizes by two electrodeposition steps[56]. In view of practical application requirements, the two layers can also be obtained by different approaches. For instance, Bao et al.[57] fabricated a porous hydrogel layer by UV-induced free radical polymerization, which was negatively charged due to the hydrolysis of carboxyl groups, and its charge density could be tuned by pH. Then, positively charged polypyrrole (PPy) was electrochemically grown on the porous hydrogel layer, and its charge density could be regulated by electrochemical stimulus (Fig. 2d). As reported, CNTs can self-assemble into a film at the air/water interface, which can achieve a steady state (hydrophobic toward the air, hydrophilic toward water) after an aging process in the air. CNTs films prepared in manners such as this can then be further modified. For example, after hydrophobic PDMS was sprayed on CNT films, a CNT/PDMS-based Janus ultrathin film with asymmetric structure, wettability, and conductivity was obtained[58].

Assembly into Janus materials based on substrates is also an effective strategy, in which the new layers can be prepared in a controlled method. Up to now, many methods appeared for unilateral deposition of new layers on substrates, including vacuum filtration[36], electrospinning[59], electrodeposition[60], hot-pressing[61], spray-coating[62], or spin-coating methods[63]. For instance, charged hydrophilic CNTs were deposited on hydrophobic PVDF membranes (Fig. 2e)[34]. By fine-tuning the composition of the filtrate, various layers with different wettability, thermal or electrical conductivity can be obtained[36,64,65]. Despite the facile, scalable, and cost-efficient nature of these approaches, optimized realization of the effective combination of layers still remains a challenge. In Fig. 2f, two kinds of responsive monomer were sprayed on each side of a fabric substrate and then polymerized and cross-linked, in which the coating layer on both sides exhibited good adhesion to the substrate[32].

2.2 In situ generation of Janus materials

The in situ generation strategy has been developed for fabrication of a single material with asymmetry, such as phase inversion, template method, interfacial polymerization, or co-extrusion, which effectively avoids the problem of weak interactions between two different layers. During the process of phase inversion in Fig. 3a, when hydrophilic components were blended in the hydrophobic matrix, water can induce hydrophilic component migration to the surface due to their strong water affinity, while the hydrophobic polymer settles at the bottom. Entanglement between molecular chains can effectively construct porous Janus materials with gradient structure, and the resulting water contact angle difference can be up to 150°, as reported by Li et al. [66]. An enormous library is available of both hydrophobic matrices and hydrophilic components. By using the co-extrusion method, Janus hollow-fiber membranes can be fabricated (Fig. 3b) [67], choosing the main matrix component, while the outer and inner layer drop solution contained different modifiers. The newly developed interfacial polymerization strategy[68] also promises to enhance the binding of separate layers by covalent connections (Fig. 3c). Due to the immiscibility of the aqueous solution and organic solution, the hydrophilic monomer can be polymerized into a hydrogel network in an aqueous solution while the hydrophobic monomer can be polymerized into an organogel network in organic solution, and the hydro/organo copolymer will be synthesized at the phase interface. However, this method is only suitable for specific monomers, which may limit its usage. In the material-forming process, the utilization and removal of the template can provide chances to construct asymmetric pore structure or sizes. For example, in Fig. 3d[35], a colloidal template was applied for Janus/gradient materials preparation. Under gradient light intensity, the gradient polymerization and deposition of methyl methacrylate (MMA) and ionic liquids (IL) in methanol were

accomplished in the template interstices, in which the PMMA segment deposited because of poor solubility. The amount of PMMA increases from top to bottom, while the PIL shows the opposite trend, leading to asymmetric wettability. After removing the template, asymmetric pore sizes were also obtained owing to the infiltration of two different monomers or polymers on the two sides. In addition, the directional crystallization of dimethyl sulfone solvent, constructed by a bidirectional temperature gradient, was induced in a polymer matrix. After removal of the solvent crystals, asymmetric pores were obtained[69], but the Janus materials' mechanical properties should be considered, and this method often involves complex procedures.

2.3 Asymmetric modification into Janus materials

Depending on the nature of the substrates, asymmetric modification can be realized by phase boundary strategies and non-phase boundary strategies, in which the interfacial weak bonding problem does not exist as mentioned in Section 2.1. Common phase boundary strategies are based on the gas-liquid boundary, solid-liquid boundary, and liquid-liquid boundary. Non-phase boundary strategies utilize the asymmetric distribution of vapor molecules, ions, or light in the dimension of porous substrates' thickness, which can create a chemical or structural gradient into the specific substrate after reaction. In practice, the two strategies can be used separately or together.

2.3.1 Phase boundary strategies

The core of this strategy is introducing a phase boundary in one single substrate to achieve asymmetric modification in the different phases. Usually, one phase contains the modifiers, while the other acts as a protective mask to prevent modification. The spatially confined feature endows differential modification on different sides of one

material substrate. For the construction of gas-liquid boundary, as displayed in Fig. 4a[70], when the hydrophobic substrate is floated on dopamine solution, the bottom surface was immersed in the solution to realize biomimetic adhesion of polydopamine coating, while the top surface was exposed in the air maintaining an unmodified interface. Dopamine, which possesses plentiful reaction sites for metal binding or organic species grafting, offers additional routes to realize various further modification[71,72]. For instance, asymmetrical CNTs films were fabricated by in situ growth of AuNPs on the PDA-coated side of CNTs film[73]. The kinds of hydrophobic substrates are also diverse, such as aerogel, PET fabric, and PP or PVDF membrane[74,75]. In addition, PMMA, which can be a solid material or hydrogel, is often applied to shield one side of a substrate from contacting the modifiers (Fig. 4c)[76]. After accomplishing asymmetric modification, the PMMA is easy to remove. Similarly, glass substrates can be used to protect one side of a CNTs membrane while the other side is grafted by hydrophobic polymer. Then, the CNTs membrane can be flipped over and deposited onto another glass substrate to achieve unilateral grafting of hydrophilic polymers[26]. Oil/water interfaces have also been explored, in which either both of the two phases can include different modifiers or only one phase contains a modifier. As reported by Shao et al. (Fig. 4b), fabric substrates can remain stable at the oil/water boundary, with the oil-contact side becoming hydrophobic while the other side in water phase remains unchanged[77]. By the phase boundary strategies, porous substrates can be easily endowed with Janus character, which can greatly broaden the application fields of the original materials.

2.3.2 Non-boundary strategies

Non-boundary strategies are effective and critical for the fabrication of the Janus materials with gradient structure. For example, Tian et al. [78] utilized the vapor of 1H,1H,2H,2H-perfluorooctyltrichlorosilane (POTS) to hydrophobize hydrophilic cotton fabric, because the abundance of reactive hydroxyl groups of the fabric can react with POTS through silanization (Fig. 4d). The existence of the fabric hindered the diffusion of the vapor, which resulted in the gradient distribution of POTS across the fabric and realized asymmetric modification. Similarly, trimethyl aluminum and water vapor can also be utilized to grow hydrophilic Al_2O_3 on the exposed surface of hydrophobic polypropylene (PP) membranes by virtue of the diffusion-controlled atomic layer deposition (ALD), in which the thickness of Al_2O_3 functionalization and the depth into the membrane pores can be tuned by controlling precursor exposure conditions and ALD cycles (Fig. 4e)[79-82]. In addition, some researchers similarly adopted ion interface diffusion to realize gradient chemical precipitation along the thickness of the membrane. With Ca^{2+} diffusing downward and PO_4^{3-} diffusing upward, the hydrophilic $Ca_3(PO_4)_2$ nanocrystals grew on the hydrophobic PVDF membrane prewetted by Ca^{2+} when these two kinds of ions came into contact (Fig. 4f)[83]. The gradient distribution of hydrophilic nanocrystals across the hydrophobic substrates' thickness leads to asymmetric wettability as well as variation of pore sizes on the two faces.

Unilateral energy irradiation, whether via laser[84], plasma (Fig. 4g)[78], or UV light, can weakly oxidize the treated surface of a hydrophobic material to generate hydrophilicity, which has the advantages of relative simplicity, short time, zero pollution, and high precision. Laser perforation can produce conical micropores for the preparation of Janus materials with asymmetric pore size or structure, and the sizes of the perforated micropores are tunable with increasing laser power. However, the technology may be

limited to the laboratory scale due to the high cost. In general, unilateral energy irradiation methods are often used as one of several sequential steps in the preparation of Janus materials. For example, Abraham et al.[85] utilized CO_2 plasma to etch one side of CNT membranes to form oxygen functional groups with subsequent vapor deposition of PDMS for stable hydrophobic silane coatings. Subsequently, the other side of the CNT membranes was etched by CO_2 plasma to obtain superhydrophilicity. In addition, since light is difficult to penetrate through the whole substrate, unilateral photo-crosslinking or photo-degradation can occur under UV irradiation to achieve asymmetry preparation[86,87]. The relative thickness of the purposed layer can be tuned by adjusting the irradiation time.

2.4 Multifunction integration into Janus materials

When Janus character is combined with functional substances, the obtained materials can present various or even intelligent performance. There are two principal strategies for fabricating this kind of multi-functional porous Janus material. One method is introducing nanomaterials as auxiliary functional materials. For instance, Wang et al.[13] conducted hydrophilic modification on a hydrophobic PTFE membrane and introduced magnetic Fe_3O_4 nanoparticles at the same time, subsequently, the top layer was peeled off to expose the hydrophobic interior to obtain Janus materials with magnetism. Similarly, when replacing with pH-responsive molecule functionalization, fabrication of Janus materials with pH-responsivity was accomplished. Another method is to directly engineer functional coatings into Janus materials. An et al.[88] functionalized the hydrophilic side of a Janus material by photo-crosslinkable gelatin methacrylate (GelMA) hydrogel, which can also serve as a platform to introduce various active compositions like growth factor to promote skin regeneration.

Owing to graphene oxide (GO)'s excellent electrical and thermal conductivity[89], researchers vaporized HI acid to induce GO reduction for constructing asymmetric wettability[29]. The obtained Janus IrGO/rGO film can effectively respond to humidity, heat, and electricity, which is a promising candidate for actuators. In addition, in combination of Janus wettability, MXene with broadband light absorption and theoretically 100% photothermal conversion efficiency exhibited excellent performance in the field of photothermal seawater desalination[30].

3 Work mechanisms of porous Janus materials

The asymmetric properties of porous Janus materials are diverse, and the duality can work independently or synergistically, which offers promise for a wide range of applications. In the synergistic working mode, the unique properties of porous Janus materials endow the ability of directional transport of liquid or bubbles and rectified ion transport, which cannot be realized by conventional homogeneous materials. Whereas in the independent working mode, porous Janus materials can be regarded as a manifestation of multifunction integration.

3.1 Synergistic mode of asymmetry

3.1.1 Directional liquid transport

Directional liquid transport can be realized easily under external forces like pressure. However, in nature, many creatures can utilize specific anisotropic interfaces to transport water directionally without consuming energy, such as certain desert beetles[90], cacti[91], or spider silk[92], in which the water droplets can be driven by gradients of chemistry, shape, or Laplace pressure. Inspired by these natural systems, porous Janus materials with asymmetric wettability have been extensively investigated to accomplish

directional liquid transport across the material's thickness without external forces[23]. As shown in Fig. 5a, a water droplet can penetrate porous Janus materials from the hydrophobic side to the hydrophilic side but will be blocked in the opposite direction. This scenario can also happen while the water droplet is fed upward[14,87,93]. In addition, oil directional transport has been realized by oleophobic/oleophilic Janus membranes in air[12], with behavior similar to the water directional transport (Fig. 5b). It is notable that the hydrophilic layer is usually oleophilic in air but oleophobic under water according to Young's equation of underwater oil contact angle[94], and the hydrophobic layer is usually oleophilic due to the low surface tension of oil. Therefore, unidirectional oil penetration can also be accomplished by hydrophobic/hydrophilic porous Janus materials under water (Fig. 5c)[11].

In order to reveal the underlying mechanisms of directional liquid transport of porous Janus materials, here we introduce surface energy analysis (taking the water droplet as an example), as reported by Long et al.[21]. The surface energy E of the water droplet on the material's surface can be expressed as follows:

$$E = X\gamma_{lv} + Y\gamma_{sv} + Z\gamma_{sl} \quad (1)$$

where X, Y, and Z are contact areas of the liquid/vapor, solid/vapor, solid/liquid, respectively; γ_{lv}, γ_{sv}, and γ_{sl} are the corresponding interfacial tensions of the liquid/vapor, solid/vapor, solid/liquid, respectively. In order to express the surface energy analysis clearly, we also define the original state, in which E_0=0 (Fig. 6a). Thus, the surface energy E_i of water droplet on the materials can be expressed as:

$$E_i = E_i - E_0 = (X_i - \mathrm{X}_0)\gamma_{lv} + (Y_i - Y_0)\gamma_{sv} + (Z_i - Z_0)\gamma_{sl} \quad (2)$$

In this situation, the increased area of water on the surface comes from the reduced surface area of the surface covered by gas, there are $Z_i - Z_0 = Y_0 - Y_i$, $Z_0 = 0$. Therefore, $E_i = (X_i - X_0 - \mathrm{Z}_i\cos\theta)\gamma_{lv}$, according to Young's formula (equation 3).

$$\gamma_{sl} + cos\theta\gamma_{lv} = \gamma_{sv} \tag{3}$$

θ is the water contact angle on the material surface. Based on the hypothesis of the droplet crown model[21], $Z_i = X_i(1 + cos\theta)/2$, $X_i^3 = (72\pi V^2)/((1 - cos\theta)(2 + cos\theta)^2)$, where V is the volume of the water droplet. Thus, the surface energy of water droplets on the materials surface can be expressed as: $E = \gamma_{lv}(9\pi V^2)^{1/3}(cos^3\theta - 3cos\theta + 2)^{1/3}$-$X_0\gamma_{lv}$. E is positively correlated with the water contact angle θ ($0° \leq \theta \leq 180°$), so the surface energy of water droplets on the hydrophobic side (E_1) is larger than that on the hydrophilic side (E_2) due to the larger θ in Fig. 6(b and c). Spontaneous directional transport of water is therefore possible, in which the water droplets would move along the energy-reducing track in the porous connected structure.

However, only when the energy barrier caused by the hydrophobic layer is overcome by the water droplet from the hydrophobic side to the hydrophilic side—but not from the opposite direction—can the water droplet realize directional transport. As shown in Fig. 6d, a water droplet on the hydrophobic side is subjected to hydrostatic pressure (P_H), intrusion pressure (P_I), and Laplace pressure of the curved surface of the water droplet on the material (P_L), which can be presented as follows[40,95,96]:

$$P_H = \frac{\rho V g}{S} \tag{4}$$

$$P_L = \frac{2\gamma_{water}}{R} \tag{5}$$

$$P_I = \frac{2\gamma_{water}cos\theta_1}{r_1} \tag{6}$$

ρ , V , and g are the density, volume, and gravitational acceleration of water droplets, respectively. S represents the contact area between the droplet and the surface. γ_{water} is the water surface tension, and R is the local radius of the water droplet on the material surface. θ_1 and r_1 are the water contact angle and average pore radius of hydrophobic layer, respectively. P_H and P_L are the inner driving force, while the P_I is the resistance. Only if the water droplets contact the bottom hydrophilic layer under the combination of these three forces can the water droplets permeate from the hydrophobic side to the hydrophilic side with the capillary force (P_C) of the hydrophilic layer coming into effect and the P_I disappearing (Fig. 6e)[87].

$$P_C = \frac{2\gamma_{water} cos\theta_2}{r_2} \quad (7)$$

θ_2 and r_2 are the water contact angle and average pore radius of hydrophilic layer, respectively. By contrast, the water droplet on the hydrophilic side was subjected to P_I, P_C, P_H, and P_L (Fig. 6f). Due to the hydrophilic property, the water droplet will exhibit a larger apparent radius, and thus lower P_L, so it is more difficult for the water droplet to overcome the energy barrier. Therefore, in terms of materials, directional liquid transport properties depend on the respective wettability (θ) and pore size (r) of both sides, the nature of the liquid (ρ, g, γ), and the liquid volume (V). The thickness of the hydrophobic layer also plays a significant role, which affects the process of the water droplets contacting the bottom hydrophilic layer. Thicker hydrophobic layers result in higher energy barrier, which is unfavorable for water droplet transport.

Electrospinning membranes, fabric, and mesh are usually used for porous Janus material fabrication to realize directional oil/water transport owing to their micron-scale pores leading to lower P_I[97-100]. Several interpretations have been proposed to unravel

the transport process in these materials. For example, Cao et al.[40] designed one Janus system composed of a ca. 3 mm high upper thin water column and a superhydrophobic mesh to realize "antigravity" water delivery. During this process, P_L was the main inner driving force, in which the effect of gravity deforms the droplet slightly, causing a small change for P_L. As shown in Fig. 7, the directional water transport was divided into four stages. $P_{L1\text{-}L4}$ represents the Laplace pressure varied by water droplet curvature, while P_{swp} is the static water pressure. During the first three stages, the water transport velocity gradually increased to its maximum owing to $P_{L1\text{-}L3} \geqslant P_{swp}$, while the speed declined to zero at the end stage ($P_{L4} < P_{swp}$). Such interesting directional liquid transport performance will find applications in various fields[26,101-103], such as advanced oil/water separation, fog collection, wound healing, and moisture management.

Although many efforts have been dedicated to the directional water transport property of porous Janus materials and significant progress has been made, most materials can only realize a small amount of water transport in a directed manner. Methods to optimize the directional liquid transport for porous Janus materials are highly desired. For example, the conical micropore array was introduced in hydrophobic/super-hydrophilic Janus textiles to enhance the directional water transport capability[18]. Conical micropore arrays, with large openings on the hydrophobic side, possess a hydrophilic inner surface. As shown in Fig 8a$_{1\text{-}2}$, a transport difference between conical micropores and cylinder microchannels embedded in the Janus textile was created. In the intrusion process, the conical micropore has a large pore diameter and thus lower P_I. In the wetting process, water in the conical micropore has a higher driving force due to the different shapes. In the transport process, the P_C derived from the super-hydrophilic layer is almost the same. During the absorption process, the conical

micropore has minimal resistant force. In all, conical micropores effectively enhance the directional transport of water. As another example, Hou et al.[104] designed amphiphobic/ superhydrophilic Janus membranes with nanoneedle/nanofiber interpenetrating structure for high unidirectional penetration performance, with a potential application in electronic liquid diodes. As displayed in Fig. 8b, compared with a common hydrophobic/hydrophilic Janus membrane (Fig. 8b$_1$), the interpenetrating structure shortened the distance between the two layers (Fig. 8b$_2$) and decreased the P_I. Therefore, water can more easily contact the underlying superhydrophilic layer to complete transport due to the reduced energy barrier. Moreover, the conical nanoneedles exhibit structure-induced Laplace pressure similar to cactus spines (Fig. 8b$_3$), which can realize self-driving water transport. In Fig. 8b$_4$, the existence of the nanoneedles did not change the penetration resistance from the superhydrophilic side to the amphiphobic side. The two methods mentioned above focused on the improvement of water transport from the hydrophobic side to the hydrophilic side. Taking a different strategy, some researchers[105] have constructed progressive wettability by introducing a transfer layer between the two layers of common porous Janus materials to obtain ultrahigh one-way transport capacity, which aimed to increase the hydrophobic layer breakthrough pressure. In Fig. 8c$_1$, water can transport from the hydrophobic side to the hydrophilic side under a wettability gradient, but the water droplets will suffer from double-blocking from the transfer layer and the hydrophobic polyurethane (PU) layer while moving from the hydrophilic side to the hydrophobic side (Fig. 8c$_2$). The different pore sizes in the hydrophobic layer and hydrophilic layer can play an important role in directional water transport[55]. In Fig. 8d$_1$, the hydrophobic layer with a larger pore size will possess a lower P_I, and the hydrophilic layer with a smaller pore size exhibits a larger P_C, both of which are beneficial to directional water

transport. In contrast, the smaller pores on the hydrophobic side will result in higher P_l, and the larger pores in the hydrophilic layer are adverse for drawing water (Fig. 8d_2). However, it is also easier for water to penetrate from the hydrophilic side to the hydrophobic side due to the increased pore size in the hydrophobic side. These methods of optimizing water directional transport performance can also be utilized to improve oil transport or that of other fluids.

Based on the directional liquid transport properties, porous Janus materials can find their unique functionality in the fields of oil/water separation, fog collection, personal moisture, and healthcare management.

Oil/water separation

There are two main strategies for oil/water separation using porous Janus materials in the synergistic working mode: collection and separation. The collection strategy is based on directional liquid transport characteristics of porous Janus materials. For water droplet collection, a Janus membrane-capped "trapper" allows water droplets through-plane penetration from the hydrophobic side to the hydrophilic side and prevents the collected water from leaking due to the repulsion of the hydrophobic layer, while the oil cannot enter into the "trapper" because it is repelled by the thick hydrophilic-underwater oleophobic layer (Fig. 9a)[78]. For interpenetrating nanoneedle/nanofiber Janus materials reported by Wang et al.[100], the water penetrates the entire Janus material along the hydrophilic channel of the nanoneedles, whose transport rate is nearly 10 times higher than previous reports. Subsequently, Yan et al.[14] utilized this unique transport channel realizing rapid extraction of water from oil. Nevertheless, due to the limited directional liquid transport capability of porous Janus materials, this collection

strategy is simple and effective for extracting the low-content liquid phase, but only targeted on a small volume of liquid.

Separation strategies often include separating low-content phase or high-content phase from emulsions. Different from the conventional "sieving effect" of porous membranes[106-108], porous Janus materials with wettability asymmetry can accomplish highly efficient separation of low-content phase relying on directional liquid transport mechanisms and break through the limitations of pore size. This kind of porous Janus material usually has a thick hydrophobic layer and thin hydrophilic layer with emulsion breakers for oil separation from oil-in-water emulsion. For the separation of ionic surfactant-stabilized emulsion, the thin hydrophilic layer of porous Janus materials usually contains negatively or positively charged species for demulsification via the charge-shielding effect (Fig. 9b), which could realize merging and directional transport of micron-scale oil droplets. Several common charged substances have been explored, such as amino or carboxylate CNTs[34], poly(diallyldimethylam-monium chloride) (PDDA)[60], poly(sodium-p-styrenesulfonate) (PSS), and poly (N,N-dimethylaminoethyl methacrylate) (PDMAEMA)[86,109]. In order to demulsify an emulsion stabilized by an ionic or non-ionic surfactant, Wang et al.[15] introduced a copolymer poly-soap into the hydrophilic layer of Janus fabric to compete with the free surfactant. The prepared Janus fabric could effectively recover oil from oil-in-water emulsion, despite the large fabric pore size of about 200 μm. Other versatile functional components, such as stimulus-responsive molecules, could be introduced into Janus materials to develop advanced oil-water separation materials.

There are few reports about Janus materials being used solely for water separation from oil-in-water emulsion, because the hydrophobic layer is easily contaminated by oil,

which will prevent water from permeating. Another novel research concept was presented by Wang et al.[12], in which they designed a superoleophobic-oleophilic membrane to speed up oil separation because the asymmetric wettability provides an inner driving force for oil transport through the membrane. However, it will be difficult for applications involving light oil separation on account of the water layer forming above the membrane.

Fog collection

Fog accounts for a substantial amount of freshwater in the world, which suspends in the atmosphere with droplet sizes ranging from 1 μm to 10 μm[110]. Inspired by plants and animals surviving in the arid regions, biomimetic fog collection technologies have been explored actively as a strategy to help alleviate water shortages. Various processes taking place during attempted fog water collection have been proposed, including rebound, evaporation, harvesting, and sliding away. In general, fog droplets on superhydrophobic materials tend to bounce back or penetrate through rather than condensing on the surface, while the droplets on hydrophilic materials are inclined to slide away under gravity once the hydrophilic materials are wetted and saturated. Janus materials with asymmetric wettability provide new strategies for dealing with this challenge, realizing higher water-harvesting capacity via quick water transport with low evaporation. According to previous reports[16,55,74], an efficient fog collector should possess: (1) droplet capture; (2) rapid transport of water; (3) relatively hydrophobic surface to regenerate; and (4) low re-evaporation rate. In Fig. 9c, a hydrophobic/hydrophilic Janus copper mesh/cotton composite was rolled and integrated as a Janus fog collector. Hydrophobic copper mesh with large pores can be conducive to water drop penetration because of the lower resistance, and regenerate the

surface for water collection and alleviate the re-evaporation rate, while hydrophilic cotton acted as an absorbent[16]. The collection rate of this Janus system is 2.4 times that of hydrophilic cotton, and 1.3 times the original mesh. In order to obtain even higher collecting efficiency, rough conical spines were integrated with Janus membranes. Conical spines can capture, transport, and coalesce tiny fog droplets directly due to the difference of Laplace pressure along the spine. The study also demonstrated that the more hydrophilic layer of the Janus membrane and a conical spine length about 2 cm possess a higher fog collection rate[111].

Using a different approach, Wu et al.[55] fabricated Janus nanofibrous membranes with large pores in the hydrophobic layer and small pores in the superhydrophilic layer, which led to a 1.7-fold increase in fog-harvesting rate. This improvement is ascribed to the large pores in the hydrophobic layer reducing the water-transport resistance due to the relatively weak hydrophobic force and the small pores in the hydrophilic layer accelerating water transport owing to the large capillary pressure. Porous materials clearly have great potential in fog harvesting, and even higher collection rates can be achieved by tuning the wettability, pore size, pore structure, or through combination with other functional materials.

Personal moisture and healthcare management

In recent years, porous Janus materials have found promising applications in moisture-wicking textiles, which could provide a more comfortable microenvironment for the human body. Moisture-wicking textiles can transmit moisture vapor and sweat rapidly because of their special wettability. Nevertheless, their low rate of water transport and evaporation necessitates further improvement to meet the requirements of body

comfort. Moreover, common moisture-wicking textiles have bidirectional water permeability, especially in high-humidity conditions, meaning that water could also be transported from the environment to the skin. The asymmetric wettability of Janus materials brings new opportunities to overcome these obstacles, which implies enormous commercialization potential for intelligent textiles. Originally, it was found that a double-face fabric with hydrophobic inner–hydrophilic outer sides exhibited good directional liquid transport properties, which is promising for application in perspiration management. Due to the material's hydrophobic feature, external water is excluded to provide a dry feeling for the body, while the hydrophilic layer plays an important role in water absorption and evaporation. In order to obtain high-performance moisture-wicking textiles, significant effort has been dedicated to designing the structure of the hydrophilic layer of the pores, as well as the intermediate transfer layer between the hydrophobic layer and hydrophilic layer. For example, Dai et al.[18] presented a novel Janus textile with hydrophilic conical micropores by laser perforation technology (Fig. 9d). Water can be transported unidirectionally from the bottom hydrophobic layer to the top super-hydrophilic layer with the conical micropores from large to small openings. Compared with cylinder microchannels and inverted conical micropores (from small to large openings) in the same Janus textiles, the large-to-small system possessed the lowest theoretical intrusion pressure, the highest driving force, and the lowest transport resistance. Another study focused on ultrahigh directional water-transport capacity, which involved construction of a wettability gradient between the hydrophilic hydrolyzed polyacrylonitrile (HPAN) layer and the hydrophobic PU layer via introduction of a transfer layer (hydrolyzed polyurethane–polyacrylonitrile, PU-HPAN)[105]. In contrast with bilayered Janus textiles (PU/HPAN), the optimized trilayered Janus textiles (PU/(PU–HPAN)/HPAN) have a 1.4-fold higher breakthrough

pressure from the super-hydrophilic side to the hydrophobic side, which is ascribed to two transfer resistances in the process. Therefore, it is difficult for environment water to penetrate through the textiles to rewet the skin, and the inner hydrophobic layer can keep completely dry. Due to the large difference in wettability between the fabric layers, sweat can be rapidly extracted from the fabric once contacting the hydrophobic layer. This moisture-wicking textile can realize continuous and spontaneous water directional transport to keep the skin dry. With the rapid development of wearable electronic devices, moisture-wicking textiles with outstanding comfort can also protect electronic products from the negative influence of body humidity[112]. In addition, temperature-responsive polymers were introduced onto different sides of cotton fabric to create Janus character. These temperature-adaptive intelligent Janus textiles generated drying and cooling effects at high temperature, with inner hydrophobic side and outer hydrophilic layer to realize directional water transport, while the Janus textiles offered thermal preservation at low temperature with outer hydrophobic side and inner hydrophilic layer. Such smart Janus textiles will have the potential in improving human comfort and reducing energy consumption caused by home air conditioners via moisture/thermal management [32].

Excess exudate around wounds provides a wet environment and hinders wound healing. Porous Janus materials can deal with this problem through the synergetic working mode. Based on the directional liquid transport property, well-designed porous Janus materials can self-pump excessive biofluid unidirectionally from the hydrophobic side to the hydrophilic side (Fig. 9e) [113]. In particular, a silver-decorated self-pumping dressing with antibacterial property has enormous potential in the wound healing process. Opportunities abound for 3D Janus materials to enhance the wound healing rate. Porous Janus materials with asymmetric wettability will also have prospects in

collecting trace blood or sweat in conducting labeling analysis to obtain human health status. For example, in Fig. 9f, Janus materials were applied into blood glucometers, which can be used for separation of blood plasma for accurate measurement of blood glucose. This membrane can transport fast microliter-quantity blood due to the inner driving force produced by asymmetric wettability, and the hydrophobic layer plays an important role in inhibiting the diffusion of blood on the membrane surface and reducing the blood amount for testing[83]. In addition, the super-amphiphobic fabric will obtain dissimilar wettability on the irradiated surface under varying unilateral UV treatment time, leading to different phenomenon of directional liquid transport to infer surface tension range of liquids.[114]

3.1.2 Directional bubble transport

Bubble manipulation is central to a number of practical applications, and directional bubble transport has been realized by porous Janus materials. In Fig. 10 (a and b), a bubble can penetrate from the aerophobic side to the superaerophilic side under water, but tends to spread horizontally in the opposite direction. The underlying mechanism here is similar to that of directional water transport across porous Janus materials, both of which are caused by asymmetric wettability. For surface energy analysis of bubbles, it is also found that the surface energy (E_i) is positively correlated with the bubble contact angle ($0° \leq \theta \leq 180°$)[21], indicating that E_i is relatively high on the aerophobic side. Therefore, as depicted in Fig. 10a, when the aerophobic side was up, there is $E_1 = E_2 > E_3 = E_4$.The bubble can be driven by Laplace pressure (P_{LW}) to pass through from the aerophobic side to the superaerophilic side (equation 8)[21].

$$P_{LW} = \gamma_{water}(1/R_1 - 1/R_2) \quad (8)$$

where γ_{water} is water surface tension, R_1 is the radius of the bubble on the aerophobic side, and R_2 is that on the superaerophilic side. Meanwhile, when the superaerophilic side is up, there is $E_3 = E_4 > E_1 = E_2$ (Fig. 10b), which explains horizontal diffusion rather than penetration of bubbles.

Sometimes directional bubble transport is necessary but insufficient for the goal of more complex transport behavior. Long and co-workers[21] further combined asymmetric wettability with a geometry gradient to realize the 3D transport of bubbles underwater. A superhydrophobic/hydrophobic (superaerophilic/ aerophobic) foam was designed to be triangular, which generates additional Laplace pressure P_{LS} (equation 9) along the surface, analogous to cactus spines.

$$P_{LS} = \gamma_{water}(1/R_r - 1/R_t) \quad (9)$$

where R_r and R_t are the bubble radius on the narrow and wide side of the foam (the left and right side of the material in Fig. 9c), respectively. When the bubbles are provided on the aerophobic side (Fig. 10d), the bubble can transport from the upper left side to the lower right side of the material under the cooperative effect of the vertical P_{LW} and horizontal P_{LS} . As a comparison, owing to the directional bubble-transport performance, when the bubbles are provided on the superaerophilic side (Fig. 10e), only P_{LS} drives the bubble moving from the left side to the right side (Fig. 10f). Efficient three-dimensional bubble transport exhibits strong application prospects in gas-involved physical or chemical processes. In the process of water-splitting to produce hydrogen and oxygen, the generated bubbles are commonly driven off the electrode by buoyancy to overcome bubble adhesion, resulting in low gas-transport efficiency. Due to the directional bubble-transport properties of porous Janus materials, an electrode

with Janus character can spontaneously transport hydrogen and oxygen from the gas-generating side to the gas-collecting side, exhibiting superior gas transport[22]. Further, as shown in Fig. 10b, porous Janus materials can transfer the generated microbubbles to the desirable site, which can realize in situ separation and spontaneous collection with high efficiency[21]. Interestingly, gas transport can be tuned to adapt to various circumstances. In particular, anti-buoyancy directional transport of bubbles can endow porous Janus materials with potential to manipulate bubbles under zero-gravity conditions. Owing to their directional bubble-transport properties, porous Janus materials can also display excellent performance in gas collection underwater with high efficiency (~15 mL cm^{-2} min^{-1}, Fig. 10h)[20].

3.1.3 Rectified ion transport

Recently, porous Janus materials composed of asymmetric charges and pores have been proposed as effective materials to realize rectifying ion transport, which show huge potential in osmotic energy conversion[115-117]. Charge asymmetry of the porous material can lead to asymmetric ion distribution in the pores according to the Donnan effect, which will result in distinguished ionic flow when applying different biases. As shown in Fig. 11a, both the cations and anions migrated toward the Janus junction under negative voltage and then accumulated in the pores due to electrostatic interactions, leading to higher ionic conductivity and then a relatively high ionic current[57]. In contrast, the pores are depleted under positive voltage thus resulting in lower ionic conductivity and a relatively low ionic current. It is worth noting that the charged pore size needs to be comparable with the Debye length of the ionic solution, which preferably allows the transport of counterions to realize ion selectivity. At higher ion concentration, the Debye length was compressed and the counterions were completely

shielded. Therefore, when the pore size in the charged layer was larger than the Debye length, no significant ionic current rectification (ICR) phenomenon can be observed. For example, Lei's group fabricated[57] hydrogel poly (acrylamide-co-acrylic acid)/ poly-pyrrole (P(AAm-co-AA)/PPy) heterogeneous membranes with the pore size of the positive PPy layer around 65 nm, obtaining a maximum ICR value of 5.7 in 1×10^{-6} M KCl solution. The rectification ratio increases with a decrease of the electrolyte concentration. In contrast, another porous Janus material with a positively charged layer with a pore size of ~8 nm and a negatively charged membrane with a pore size of ~17 nm can realize ion rectification in a hypersaline environment (the maximum rectification ratio appears at 1 M KCl) [25]. The charge density within porous Janus materials also affects the ion concentration in pores, which is critical in ICR. The higher surface charge density benefits the conductance and enables optimized rectification.

In Fig. 11b [118], compared with the small amount of negative charges on the bottom side, the upward side positively charged layer plays a dominant role in the ion selectivity. Therefore, ionic transport across the porous Janus material will take place in an asymmetric electrolyte solution. When the porous Janus material is placed between KCl solutions of different concentrations, the concentration difference makes Cl^- diffuse to the low concentration side and the generated concentration polarization is minimized by its surface negative charge-induced electrostatic repulsion, assuring highly efficient ion-selective transport. The continuous asymmetric ion diffusion generated potential between the two sides of porous Janus materials results in electrochemical redox reactions on electrodes and electron transfer in external circuits. In this way, the osmotic energy can be harvested for electricity generation by virtue of the porous Janus materials. Compared with conventional materials, bipolar porous Janus materials can address the problem of ionic concentration polarization on the material's surface toward

the low concentration solution and possess ion selectivity that can work as a diode[119-121]. As reported by Lei's group, a porous Janus membrane with tunable surface charge density and narrow pore-size distribution has excellent anion selectivity and ionic rectification, which can work for a long time maintaining high performance. A series of these Janus membranes can be connected as a generator, which has been demonstrated to power a calculator for 120 hours [25].

The Poisson and Nernst−Planck (PNP) equations are widely adopted for evaluating ionic rectification of these Janus materials. As shown in Fig. 11c(1) and c(3)[118], distinguished with rectification failure of the homogeneous porous materials, Janus materials exhibit remarkable ion depletion and ion accumulation effects, indicating apparent ionic rectification.

3.2 Independent mode of asymmetry

The asymmetric faces of porous Janus materials can work independently of each other, which can integrate several functions together and optimize the practical application process to obtain superior performance relative to traditional homogeneous materials.

Water purification

For oil/water separation discussed in section 3.1.1, porous Janus materials adopt directional liquid transport properties by finely adjusting the thickness of the asymmetric layers. In contrast, in this section, the porous Janus materials usually have similar thickness of the hydrophilic and hydrophobic layers, which can work independently to exhibit the performance of solely hydrophobic and hydrophilic membranes to realize both water-in-oil and oil-in-water emulsion separation just by

converting the material's corresponding wetting surface to face toward different emulsions[26,64,65]. Compared with traditional separation or adsorption materials completing only one emulsion separation or single-phase adsorption[122-125], porous Janus materials exhibit superiority. Owing to the lower surface tension of oil, both layers of the porous Janus material can be wet by oil. Thus, porous Janus materials will exhibit high oil-separation efficiency and flux under low pressure for water-in-oil emulsion, when the hydrophobic layer faces the emulsion. Therefore, in order to allow water from oil-in-water emulsion to pass through, the hydrophilic layer needs to face the emulsion and its underwater oleophobicity can repel oil. However, the existence of a hydrophobic layer at the bottom is not conducive for water to pass through, which will result in low flux or require external pressure to accomplish separation. In addition, three-dimensional (3D) porous materials, with micron-scale pores and ultrahigh porosity, like aerogels, foams, and sponges[126-128], as effective candidate substrates for Janus character construction, can be applied for various oil/water emulsion separation with high flux as well as high rejection just under the driving force of gravity (Fig. 12a)[70].

Porous Janus materials with improved interfacial floatability have received increasing attention[129]. Therefore, in addition to serving as a separation material, porous Janus materials can also exhibit excellent gating properties for various oil/water separations. As reported by Li's group, liquid-based porous Janus materials were prepared through infusion of water and oil within the hydrophilic layer and hydrophobic layer, respectively. As shown in Fig. 12b, these Janus materials can exhibit excellent buoyancy at the oil-water interface, and self-gating behavior will exhibit when the separation process is completed.[130]

Nanofiltration is an important membrane separation technology, which is used to separate small molecular organic compounds with molecular weight between 200 and 1000 Da as well as high-valence salt ions[131-133]. When the nanofiltration membrane is coupled with Janus character such as counter charge, it can intercept ions or dyes with a positive or negative charge simultaneously[134-137] or separate of ions with different valence states[138]. Interfacial polymerization has been widely used for the preparation of nanofiltration membranes, which is also promising for the construction of asymmetric properties as described in Section 2.2. When the aqueous monomers and oil monomers possess ionizable groups, a Janus film with asymmetric charges can be obtained. For example, a Janus polyamide (PA) nanofilm for nanofiltration was prepared via reaction of amines and acyl chlorides. One side of the as-obtained PA layer is rich in amine groups that can be protonated to show positive charge, while the other side contains abundant carboxyl groups that can be dissociated and negatively charged. The charge properties can be tuned by regulating the concentration of amine and acyl chloride. High rejection of Mg^{2+} and SO_4^{2-} were both achieved without compromising permeability (Fig. 12c)[139].

In addition, organic solvent nanofiltration (OSN) is an important research direction of nanofiltration technology that aims to separate small compounds from organic solvents to realize the recovery and reutilization of organic solvents, which is important for utilization of resources and environmental protection[140,141]. Poor solvent resistance of materials and low permeability flux are major challenges in this field[142]. Distinguished from conventional solutions such as thickness minimization and inter-spacing maximization[143-145], creating Janus character within a membrane provides new routes for the design of highly efficient nanofiltration membranes. Wang et al.[146] designed hydrophilic/hydrophobic heterostructures to improve the permeability of nonpolar or

polar solvents and maintain high rejection of several dyes. Hydrophobic polydimethylsiloxane (PDMS) clusters were constructed on hydrophilic GO and improved the permeance of n-hexane and toluene by over 7 and 10 times, respectively. The hydrophobic PDMS cluster is conducive to absorbing nonpolar solvents, and the GO layer has weak molecule-channel interactions with nonpolar molecules to enable rapid transport. Similarly, patterning hydrophilic chitosan (CS) clusters on hydrophobic reduced graphene oxide (rGO) can improve polar solvent transport such as water and acetone. To realize the sieving of both polar and nonpolar molecules by one membrane, Janus pathways were proposed with hydrophobic inner cavities and hydrophilic channels though the interfacial reaction between cyclodextrin (CD) and trimesoyl chloride (TMC)[147].

Membrane distillation (MD), a phase-change separation process, is an effective way to desalinate hypersaline brine water or wastewater driven by steam pressure difference under atmospheric pressure and lower operating temperature. In MD, a membrane exists between the hot feed solution and cool distilled solution, so that the water vapor is directed through the membrane pore from the high-vapor-pressure side (hot feed liquid side) to the low-vapor-pressure side (cool distilled liquid side)[148]. Traditionally, membranes used for MD are hydrophobic[149], such as polypropylene (PP), polyvinylidene fluoride (PVDF), and polytetrafluoroethylene (PTFE), and their pore sizes are usually 100 Å to 1 μm, ensuring vapor flux and preventing liquid penetration. Common methods to improve MD performance are to speed up steam transfer and to reduce the heat transfer to maintain the driving force caused by the vapor pressure gradient, which is affected by the temperature difference between the two sides. Mass transfer takes place in the membrane pore, while the heat transfer mainly occurs through

the membrane matrix due to the matrix's higher heat-transfer coefficient than vapor. For hydrophobic membranes, thinner membranes showcase high mass and heat transfer simultaneously while thick membranes display low mass and heat transfer. Thus, the MD efficiency is low and limited. To address this dilemma, Janus character provides new opportunities, as shown in Fig. 12d. Hydrophobic/hydrophilic porous Janus materials can shorten the distance of vapor transmission to reduce the mass-transfer resistance and keep the high heat-transfer resistance when the hydrophilic layer contacted with the feed. Yang et al.[150] co-deposited polyethyleneimine (PEI) and dopamine (DA) on hydrophobic polypropylene hollow fiber membranes (PPHFMs) to form a hydrophilic thin layer via co-deposition, in which the thickness of the hydrophilic layer can be tuned by the deposition time. With the increase of deposition time, the water flux displayed an obvious upward trend (up to 120%), which is ascribed to the increase of thickness of the hydrophilic layer from 0 to 90 μm and the decrease of the thickness of the hydrophobic layer accordingly reducing the distance of the mass transfer. In addition, with the thin (30–60 μm) hydrophobic layer toward the feed, the hydrophilic layer was utilized to support a functional hydrophobic layer, which can also highly enhance the water flux, as reported by Chung's group[67].

In practical MD processes, the membrane usually suffers from fouling owing to contaminants in the feed[151,152]. Some contaminants like surfactants may be adsorbed on the membrane making it amphiphilic, and therefore the feed solution can permeate the membrane, resulting in reduced salt rejection and distillate purity. Common hydrophobic membranes in MD are also inclined to be attached by hydrophobic contaminants (e.g., humic acid (HA)) due to hydrophobic interaction, resulting in pore blockage and flux decline. Unlike the fouling-control methods of pretreatment and

membrane cleaning, Janus membranes with asymmetric wettability can be anti-fouling to improve the efficiency of MD, with the hydrophilic layer repelling the hydrophobic foulants, and omniphobic layer anti-wetting. For example, Li et al.[153] fabricated a hydrophilic /omniphobic Janus membrane with excellent anti-fouling and anti-wetting properties toward pure water, surfactant, ethanol, and crude oil, which can deal with multi-component saline wastewater. However, an omniphobic layer with lower surface energy cannot be fabricated easily. Chen et al.[154] presented a novel solution implementing an ultrathin dense nanoporous hydrophilic layer on top of a hydrophobic substrate to sieve out the surfactants in the feed solution, thereby protecting the hydrophobic substrate from being wetted, which simplifies the preparation process of Janus membranes with anti-fouling and anti-wetting properties and is of significance for the commercialization of Janus membranes in MD. Overall, constructing Janus wettability is highly promising for enhancing membrane distillation performance in practical applications.

Solar steam generation has attracted tremendous attention as a potential way to obtain clean water to alleviate water stress and reduce wastewater volume. Although various photothermal materials have been developed and work well, photothermal materials combined with Janus properties will often manifest higher desalination performance and long-term stability[155]. Asymmetric wettability was the first Janus property introduced in this arena. As shown in Fig. 12e, a hydrophobic PMMA layer with carbon black (CB) nanoparticles floated above the air/water interface for photothermal conversion and water evaporation, while the hydrophilic PAN layer remained underwater for water supply and salt crystallization resistance[156]. The CB/PMMA layer can absorb light, convert it to heat, and insulate the bulk water, which effectively reduces heat loss during steam generation. Meanwhile, the hydrophilic PAN layer can

pump water continuously and dissolve the deposited salts simultaneously due to its hydrophilic properties, which addresses the problems of salt crystallization and channel blockage on the absorber, and realizes stable desalination.

MXenes offer promise in solar steam generation due to their broadband light absorption and theoretical 100% photothermal conversion efficiency. Combined with Janus character, Zhang et al.[30] designed Janus MXene-based aerogels for highly efficient solar desalination. The upper hydrophobic layer of the Janus aerogel provided light absorption and steam escape, and the hydrophilic layer delivered water supply and inhibition of aforementioned salt crystallization. Optimal performance was achieved at the thickness value of 180 μm. A thicker hydrophobic layer was not conducive to vapor escape and heat transfer, while a thinner hydrophobic layer with only partial hydrophobicity will led to salt accumulation on its walls. Advancing this field further, porous Janus materials with opposite wettability and asymmetric conical pores were utilized to enhance solar desalination performance. Due to the multi-scattering effect of the pore structure, the solar energy absorptivity is significantly improved. Under the condition where a thermal insulator prevents heat loss, the light absorbance can be up to 97% and the conversion efficiency reaches 90.2%, which is among the higher performance materials[69]. In addition, Xiao et al. prepared a Janus (CNT) film/cellulose paper with PDMS partial decoration for the combination of solar desalination and electricity generation, which represents a new approach for the development of solar-thermal-electro systems[157]. Optimization of solar desalination performance of Janus structures is still in the primary stage, and further efforts should be made for the application of this material in practical settings.

Beyond the applications discussed above, porous Janus materials also have important application prospects in forward osmosis (FO) and membrane catalysis. In FO, the hydrophilic porous layer provides a mechanically stable low-fouling support to the hydrophobic layer, while the hydrophobic layer offers a blocking barrier for reverse ion diffusion. Liu's group[59] proposed a diffusion-evaporation-condensation mechanism for the mass transfer of porous Janus materials in FO processes, which is different from the classical solution-diffusion model. According to this mechanism, water molecules first rapidly diffuse into the hydrophilic layer, evaporate into steam, pass through the air gap of the hydrophobic layer, and then condense on the liquid draw solution side. The obtained porous Janus materials exhibited high water flux and low reverse salt flux. Janus character have also been applied to catalytic membrane reactors[158]. For example, a Janus membrane composed of a TiO_2 catalyst layer on a superhydrophobic carbon fiber film can greatly enhance its photocatalytic reactivity due to the hydrophobic layer promoting diffusion of oxygen to the catalyst surface, in which the degradation rate was increased by nearly 12 times (Fig. 12e) [159].

Sensor devices

Inspired by nature, materials with shape transformations have elicited extensive research interest for potential in sensors. There are two principal methods to realize the design of these materials: one is to design complex patterned films with local active components, the other is to construct bilayer films relying on different responses of each layer to stimuli such as humidity, light, and heat. Shape transformations can be easily achieved by using the difference of swelling degree of different porous polymer networks in solvent. For example, Zhang et al.[68] designed hydrogel/organogel Janus film via interfacial polymerization. The hydrophilic PAA hydrogel is covalently

connected with the hydrophobic PBMA organogel (Fig. 13a). In water, the PAA hydrogel is easier to swell and deform due to its hydrophilicity, but the PBMA organogel exhibits water repellency and almost no deformation, resulting in bending toward the side of the organogel. However, when in the oil phase, the Janus film bends toward the PAA hydrogel because the oil can expand the PBMA organogel but is repelled by the PAA hydrogel. This Janus film therefore achieves bidirectional bending under the binary synergistic effect of hydrogel and organogel. The two layers of porous Janus materials with asymmetric wettability can have different sensitivity to vapor, which will lead to different deformation and actuation effects. The hydrophilic layer is sensitive to water vapor for inflation, while the hydrophobic layer is stable. The Janus film reverts to the original flat conformation when both sides are full wet.

When well-ordered periodic structures are introduced into a Janus film, structure color/optical signal alteration can take place during the actuation process, which can be utilized to monitor the actuation behavior (Fig. 13b)[35]. Multi-responsive Janus actuation has also been developed. Graphene has been receiving broad attention due to its superior structure and electrical/thermal conductivity, which can be used for smart materials when combined with Janus properties. For instance, Yang et al.[29] fabricated Janus iodine-doped reduced graphene oxide (IrGO)/rGO films via unilateral gradient reduction of GO films, which can respond to humidity, heat, and electricity. With different reduction degrees, the Janus films also have asymmetric wettability and water adsorption capability, resulting in film deformation. Heat can affect water adsorption and desorption, while electricity can be converted into heat. In general, Janus wettability of the films plays a vital role in the actuation behavior.

Other functional materials, combined with Janus wettability to facilitate multi-functional development of sensors, remain to be developed. In the field of gas sensing, it is relatively easy to realize single-gas detection, but sensing of complex gas mixtures is both more difficult and more valuable in real-world applications. Porous Janus materials could offer a promising platform in this arena due to their asymmetric properties, in which different dual active sites can simultaneously sense different gases without interference. Janus character brings opportunities for detecting multiple chemical gases in one unit (Fig. 13c)[160]. The Janus CNT/PDMS film can combine hydrophilic, conductive, and film-forming properties of CNTs with the adhesion, elasticity, and hydrophobicity properties of PDMS for the preparation of elastomer-based electronic skin, which can be used for small deformation or air-pressure detection (Fig. 13d)[58].

Biomedical applications

Wound healing is a common concern in the medical community, in which wound dressings play a critical role in everything from ordinary wounds to surgery[161]. Traditionally, cotton gauze is used for hemostasis due to its strong ability to absorb blood and stop bleeding (Fig. 14a)[162]. However, hemostatic materials based on the mechanism of absorbing blood usually adhere to and clot with the wound tissue during the healing process, which will tear the wound when changing the dressing. Furthermore, these materials often fail to prevent bacterial infection and cause excessive bleeding and wound overhydration. Based on the two working modes of porous Janus materials, they can provide innovative strategies for accelerating wound healing. In the independent working mode, for instance, researchers functionalized the hydrophilic layer of a Janus membrane with asymmetric wettability via integration of

hydrogel for wound skin regeneration[88]. This membrane-hydrogel composite Janus material displayed dual functions where the hydrogel side provided therapeutic condition promoting tissue regeneration and the superhydrophobic side had antibacterial and waterproof properties to protect the wound from damage. This versatility is difficult to realize by traditional materials.

Another potential application is to guide bone regeneration. After bone damage, it usually takes a long time to fully restore the original structure and function of the tissues. Meanwhile, the surrounding fibroblast in-growth can also deteriorate the bone defect. As reported by Lei et al.[56], a dense/ porous Janus scaffold composed of chitosan/hydroxyl apatite (HAp) composite promotes new bone tissues and bone mineral density (Fig. 14b). The dense layer was clearly seen, which can prevent the infiltration of fibroblasts and act as a mechanical support, while the high specific surface area of the porous layer is helpful to release Ca^{2+}, promote osteogenic differentiation, and bind proteins to promote cell adhesion, migration, and continuous proliferation. The results indicated the Janus composite scaffold exhibited a higher ability to guide bone regeneration. In another example, a novel Janus hydrogel wet adhesive with strikingly distinct adhesive and non-adhesive properties on its two sides can replace traditional surgical sutures and realize internal tissue/organ repair and simultaneous post-operative anti-adhesion (Fig. 14c)[76].

Other emerging applications

Polydimethylsiloxane (PDMS) is a common, inexpensive, and widely used material[163,164]. In practice, lightly cross-linked PDMS is soft and sticky possessing poor mechanical properties, while highly cross-linked PDMS is hard but non-viscous.

Recently, Wan et al. fabricated Janus adhesive tape with asymmetrically cross-linked PDMS network, in which the lightly cross-linked side has high adhesion whether in wet or dry conditions while the highly cross-linked side can act as a supporting layer with high mechanical strength[165]. As displayed in Fig. 15a, the lightly cross-linked layer (the red side with the ratios 50:1 for the silicone base and curing agent) exhibited good adhesion properties, while the transparent side for highly cross-linked layer with the ratios 20:1 was less sticky.

Battery separators are critical to the performance of electrical energy storage devices, the main roles of which are to isolate the positive and negative poles and provide ion channels[166-168]. Oh et al. designed a new class of Janus battery separator with integrated ion/electron-conductivity and chemical activity on its two sides, respectively, which was composed of a SiO_2/PVP/PAN layer and PEI/CNT layer. The thiophenyl groups on the surface of PVP/PAN/SiO_2 particles can effectively capture heavy metal ions like Mn^{2+} in the electrolyte, while the PEI/CNT layer has good conductivity, which can improve the electron conduction behavior on the cathode surface (Fig. 15b)[169]. Compared with a traditional polyethylene (PE) battery separator, the novel Janus separator significantly reduced heavy metal ion deposition on the anode surface and promoted the redox reaction kinetics, which exhibits improvement in the cell performance.

Fine-bubble aeration can increase gas-liquid contact area to promote mass transfer, which has a wide range of uses in wastewater treatment, industry, and agriculture[170,171]. Waldman et al. utilized porous Janus materials with asymmetric wettability to decrease the size of air bubbles effectively during aeration due to the existence of a superaerophobic layer facilitating bubble detachment (Fig. 15c)[79]. Moreover, the

prepared aerophilic/ superaerophobic porous Janus materials exhibited lower intrusion pressure than hydrophilic membranes because the hydrophobic layer of the porous Janus material can entrap gas in the pores. Under a similar principle, oil can behave like bubbles to pass through underwater oleophilic/oleophobic porous Janus materials under pressure to produce oil-in-water emulsion, while the water can penetrate hydrophobic/hydrophilic materials to generate water-in-oil emulsification (Fig. 15d)[27]. It is noteworthy that the hydrophobic/hydrophilic properties are usually oleophilic/oleophobic and aerophilic/aerophobic under water[94,171], enabling various advanced transport phenomena.

4 Summary and Outlook

In this review, recent research progress of porous Janus materials is reviewed, including various asymmetry and fabrication methods, unique properties, underlying mechanisms, and diverse applications. Construction of porous Janus materials, based on substrate or substrate-free methods, as well as the combination of Janus character and functional substances, is presented, including four distinct fabrication strategies. Apart from porous Janus materials with multifunction integration, well-designed systems can exhibit unique directional liquid, bubble transport, or rectified ion transport properties, the underlying mechanisms of which have been discussed. Compared with traditional homogeneous materials, porous Janus materials can showcase higher performance and enhanced energy efficiency owing to the synergistic or independent effects of duality, which inspire burgeoning interest from both traditional and emerging fields.

The development of porous Janus materials is still in its infancy, and challenges and outlook are presented as follows: (1) Many asymmetric properties have been investigated extensively, such as wettability, charge, pore size and structure, infrared emissivity, thermal or electrical conductivity, etc., but novel asymmetric properties still need to be exploited; (2) The unique properties of porous Janus materials can be expanded beyond directional liquid or bubble transport and rectified ion transport. The synergistic effect of duality should be further optimized by regulating material properties; (3) In-depth understanding and derivative theoretical fabrication guidance of directional liquid or bubble transport and rectified ion transport are needed, which are essential to realizing practical applications; (4) At present, most porous Janus materials consist of two layers, but the interfacial weak bonding affects their stability and durability. The fabrication of single materials with asymmetric properties is usually complex and cannot be precisely controlled. Therefore, low-cost, easy-to-scale production processes and technology are urgently needed for industrialization/commercialization; (5) Integration of various asymmetric properties in one Janus system is promising for multi-purpose applications; (6) Combination of Janus character with various functional materials still needs to be explored in more areas for superior performance, which may provide a way to break “trade-off” effects in some fields; (7) Introduction of Janus materials into electronic detection can exploit smart analysis and control devices; (8) 3D/4D additive printing technology may greatly promote the rapid development of novel Janus systems, but the material compositions and integration must be delicately controlled for achieving the ideal asymmetric architecture or function.

Porous Janus materials can serve as a platform for performance optimization or utilization of novel applications in various fields. In view of the above challenges in

their development, more effort is still needed to promote practical use. At present, most studies focus on the asymmetric properties of the porous Janus materials on their two faces, but more attention will be needed on the internal distribution and composition of these porous materials. New types of porous Janus materials are being explored around the world, and there are undoubtedly exciting properties and applications that will reach beyond the vision laid out in this review.

Conflicts of interest

There are no conflicts to declare.

Acknowledgements

This work was supported by the National Natural Science Foundation of China (21878062), the Natural Science Foundation of Heilongjiang Province for Distinguished Young Scholars (JQ2020B001), Heilongjiang Touyan Team (HITTY-20190033) and State Key Laboratory of Urban Water Resource and Environment (Harbin Institute of Technology) (No. 2020DX02). S.B.D. was supported as part of the Advanced Materials for Energy-Water Systems (AMEWS) Center, an Energy Frontier Research Center funded by the U.S. Department of Energy, Office of Science, Basic Energy Sciences.

Notes and references

1. Bae, S. H.*, et al.*, *Nat. Mater.* (2019) **18** (6), 550.
2. Liu, Z.*, et al.*, *Chem. Soc. Rev.* (2016) **45** (3), 460.
3. Zhang, Y. Z.*, et al.*, *Chem. Soc. Rev.* (2020) **49** (20), 7229.
4. Sheng, Z. Z.*, et al.*, *Chem. Soc. Rev.* (2020) **49** (22), 7907.
5. Yang, W.*, et al.*, *Nat. Commun.* (2019) **10** (1), 5541.
6. Yeung, T.*, et al.*, *Science* (2008) **319** (5860), 210.

7. Gennes, P.-G. d., *Angew. Chem. -Int. Ed.* (1992) **31**, 842.
8. Pang, X. C.*, et al.*, *Angew. Chem. -Int. Ed.* (2014) **53** (22), 5524.
9. Liang, F. X.*, et al.*, *Adv. Mater.* (2014) **26** (40), 6944.
10. Wang, H.*, et al.*, *J. Mater. Chem.* (2010) **20** (37), 7938.
11. Yang, X. B.*, et al.*, *J. Membr. Sci* (2018) **549**, 67.
12. Wang, H. X.*, et al.*, *Adv. Mater. Interfaces* (2015) **2** (4), 1400506.
13. Wang, Z. X.*, et al.*, *Mater. Horiz.* (2017) **4** (4), 701.
14. Yan, L. L.*, et al.*, *Chem. Commun.* (2020) **56** (3), 478.
15. Wang, Z.*, et al.*, *Angew. Chem. Int. Ed.* (2017) **56** (42), 12892.
16. Cao, M.*, et al.*, *Small* (2015) **11** (34), 4379.
17. Zhang, X.*, et al.*, *J. Membr. Sci* (2021) **620**, 118853.
18. Dai, B.*, et al.*, *Adv. Mater.* (2019) **31** (41), e1904113.
19. Chen, J. W.*, et al.*, *Chem. Commun.* (2015) **51** (59), 11872.
20. Zhu, S. W.*, et al.*, *ACS Appl. Mater. Interfaces* (2020) **12** (15), 18110.
21. Long, Z. Y.*, et al.*, *Adv. Mater.* (2020) **32** (17), 1908099.
22. Sheng, S.*, et al.*, *ACS Appl. Mater. Interfaces* (2020) **12** (20), 23627.
23. Zhao, Y.*, et al.*, *Small* (2017) **13** (4), 1601070.
24. Yang, H. C.*, et al.*, *Adv. Mater.* (2018) **30** (43), e1801495.
25. Zhu, X. B.*, et al.*, *Sci. Adv.* (2018) **4** (10), eaau1665.
26. Gu, J. C.*, et al.*, *ACS Appl. Mater. Interfaces* (2014) **6** (18), 16204.
27. Wu, M. B.*, et al.*, *ACS Appl. Mater. Interfaces* (2017) **9** (6), 5062.
28. Zhou, Q.*, et al.*, *J. Colloid Interf Sci.* (2021) **592**, 77.
29. Yang, J.*, et al.*, *Nano Energy* (2018) **53**, 916.
30. Zhang, Q.*, et al.*, *ACS Nano* (2019) **13** (11), 13196.
31. Jian, H. W.*, et al.*, *Sep. Purif. Technol.* (2021) **264**, 118459.
32. Wang, Y. F.*, et al.*, *Adv. Funct. Mater.* (2020) **30** (6), 1907851.
33. Sun, J.*, et al.*, *Langmuir* (2018) **34** (23), 6653. DOI: 10.1021/acs.langmuir.7b04339.
34. An, Y. P.*, et al.*, *ACS Appl. Mater. Interfaces* (2018) **10** (11), 9832.
35. Zhang, D. J.*, et al.*, *ACS Nano* (2018) **12** (12), 12149.
36. Yue, X. J.*, et al.*, *Nano Energy* (2019) **63**, 103808.
37. Zhou, H., and Guo, Z., *J. Mater. Chem. A* (2019) **7** (21), 12921.
38. Walther, A., and Muller, A. H. E., *Chem. Rev.* (2013) **113** (7), 5194.
39. Sheng, W. B.*, et al.*, *Angew. Chem. -Int. Ed.* (2019) **58** (35), 12018.
40. Cao, M.*, et al.*, *Adv. Funct. Mater.* (2015) **25** (26), 4114.
41. Tsai, P., *Eng. Sci.* (2020) **10**. DOI:10.30919/es8d1110.
42. Lv, D.*, et al.*, *ACS Appl. Mater. Interfaces* (2019) **11** (38), 35511.
43. Ge, J. L.*, et al.*, *Adv. Funct. Mater.* (2018) **28** (10), 1705051.
44. Yang, P.*, et al.*, *ES Mater. Manuf.* (2020) **7**. DOI: 10.30919/esmm5f618.
45. Zhang, S. Q.*, et al.*, *Chem. Eng. J.* (2020) **390**, 124523.
46. Yue, Y. P.*, et al.*, *J Colloid Interf Sci* (2021) **592**, 310.
47. Wu, J. D.*, et al.*, *J. Mater. Chem. A* (2018) **6** (16), 7014.
48. Görgün, N.*, et al.*, *Adv. Compos. Hybrid Mater.* (2019) **2** (3), 423.
49. Hou, L. L.*, et al.*, *Adv. Funct. Mater.* (2018) **28** (49), 1801114.
50. Deng, L., and Zhang, H., *ES Food Agrofor.* (2020) **2**. DOI:10.30919/esfaf1120.
51. Gao, C.*, et al.*, *Eng. Sci.* (2020) **9**. DOI: 10.30919/es8d905.
52. Zuo, B.*, et al.*, *Adv. Compos. Hybrid Mater.* (2019) **2** (2), 361.
53. Elayappan, V.*, et al.*, *Eng. Sci.* (2020) **10**. DOI:10.30919/es5e1007.
54. Wu, J.*, et al.*, *Soft Matter* (2012) **8** (22), 5996.
55. Wu, J.*, et al.*, *Adv. Mater. Interfaces* (2019) **6** (5), 1801529.
56. Lei, M.*, et al.*, *Adv. Funct. Mater.* (2019) **29** (18), 1900065.

57. Bao, B.*, et al.*, *Adv. Mater.* (2017) **29** (44), 1702926.
58. Xiao, P.*, et al.*, *ACS Nano* (2019) **13** (4), 4368.
59. Zhou, S. H.*, et al.*, *Environ. Sci. Technol. Lett.* (2019) **6** (2), 79.
60. Yang, J.*, et al.*, *J. Mater. Chem. A* (2019) **7** (13), 7907.
61. Chen, Y. F.*, et al.*, *Angew. Chem. -Int. Ed.* (2016) **55** (10), 3419.
62. Wang, H.*, et al.*, *Appl. Surf. Sci.* (2018) **455**, 924.
63. Soz, C. K.*, et al.*, *ACS Appl. Mater. Interfaces* (2018) **10** (43), 37478.
64. Hu, L.*, et al.*, *J. Mater. Chem. A* (2015) **3** (46), 23477.
65. Yang, J.*, et al.*, *J. Membr. Sci* (2018) **563**, 326.
66. Li, T.*, et al.*, *ACS Appl. Mater. Interfaces* (2018) **10** (29), 24947.
67. Bonyadi, S., and Chung, T. S., *J. Membr. Sci* (2007) **306** (1-2), 134.
68. Zhang, F.*, et al.*, *NPG Asia Mater.* (2017) **9** (5), e380.
69. Yu, H. H.*, et al.*, *Research* (2020) **2020**, 3241758.
70. Li, Y.*, et al.*, *ACS Appl. Mater. Interfaces* (2019) **11** (40), 36638.
71. Lee, H.*, et al.*, *Science* (2007) **318** (5849), 426.
72. Wang, Z.*, et al.*, *Chem. Commun.* (2020) **56** (80), 12045.
73. Zhang, L.*, et al.*, *Adv. Mater. Interfaces* (2016) **3** (15), 1600170.
74. Wang, Z.*, et al.*, *J. Membr. Sci* (2020) **601**, 117954.
75. Wang, Z.*, et al.*, *J. Membr. Sci* (2018) **566**, 161.
76. Cui, C. Y.*, et al.*, *Adv. Funct. Mater.* (2020) **30** (49), 2005689.
77. Yang, X. B.*, et al.*, *J. Membr. Sci* (2019) **576**, 9.
78. Tian, X. L.*, et al.*, *Adv. Funct. Mater.* (2014) **24** (38), 6023.
79. Waldman, R. Z.*, et al.*, *Adv. Mater. Interfaces* (2018) **5** (15), 1800658.
80. Ahvenniemi, E.*, et al.*, *J. Vac. Sci. Technol. A* (2017) **35** (1), 010801.
81. Yang, H. C.*, et al.*, *ACS Nano* (2018) **12** (8), 8678.
82. Yang, X. B.*, et al.*, *Adv. Funct. Mater.* (2020) **30** (15), 1910062.
83. Zhang, W.*, et al.*, *J. Mat. Chem. B* (2017) **5** (25), 4876.
84. Yin, K.*, et al.*, *ACS Appl. Mater. Interfaces* (2018) **10** (37), 31433.
85. Abraham, S.*, et al.*, *Adv. Mater. Interfaces* (2016) **3** (18), 1600445.
86. Wang, Z. J.*, et al.*, *Angew. Chem. -Int. Ed.* (2016) **55** (4), 1291.
87. Zhou, H.*, et al.*, *Scientific reports* (2013) **3**, 2964.
88. An, Y. H.*, et al.*, *Adv. Healthc. Mater.* (2017) **6** (5).
89. Nidamanuri, N.*, et al.*, *Eng. Sci.* (2020) **9**. DOI: 10.30919/es8d128906.
90. Parker, A. R., and Lawrence, C. R., *Nature* (2001) **414** (6859), 33.
91. Ju, J.*, et al.*, *Nat. Commun.* (2012) **3** (1), 1247.
92. Zheng, Y. M.*, et al.*, *Nature* (2010) **463** (7281), 640.
93. Yang, S.*, et al.*, *Appl. Phys. Lett.* (2018) **113** (20), 203701.
94. Yong, J. L.*, et al.*, *Chem. Soc. Rev.* (2017) **46** (14), 4168.
95. Lefevre, B.*, et al.*, *J. Chem. Phys.* (2004) **120** (10), 4927.
96. Cao, H.*, et al.*, *Appl. Surf. Sci.* (2017) **412**, 599.
97. Zhou, H.*, et al.*, *Adv. Mater. Interfaces* (2016) **3** (17), 1600283.
98. Zeng, C.*, et al.*, *Adv. Mater. Interfaces* (2016) **3** (14), 1600036.
99. Zhang, J. C.*, et al.*, *J. Mater. Chem. A* (2019) **7** (35), 20075.
100. Wang, Z. C.*, et al.*, *Chem. Commun.* (2018) **54** (78), 10954.
101. Zhong, L. S.*, et al.*, *J. Mater. Chem. A* (2019) **7** (14), 8405.
102. Guo, T. Q.*, et al.*, *Rsc Adv.* (2015) **5** (107), 88471.
103. Zhang, Q. Y.*, et al.*, *ACS Nano* (2020) **14** (6), 7287.
104. Hou, L. L.*, et al.*, *ACS Nano* (2019) **13** (4), 4124.
105. Miao, D. Y.*, et al.*, *Small* (2018) **14** (32).
106. He, S.*, et al.*, *AIChE Journal* (2020) **66** (10)..

107. Yang, X. B.*, et al.*, *J. Membr. Sci* (2020) **612** .
108. Kordjazi, S.*, et al.*, *Adv. Compos. Hybrid Mater.* (2020) **3** (2), 167.
109. Wang, Z. J.*, et al.*, *Angew. Chem. Int. Ed.* (2016) **55** (47), 14610.
110. Klemm, O.*, et al.*, *Ambio* (2012) **41** (3), 221.
111. Zhou, H.*, et al.*, *Small* (2018) **14** (27), 1801335.
112. Yang, W. F.*, et al.*, *Nat. Commun.* (2019) **10**. DOI:10.1038/s41467-019-13569-5.
113. Shi, L. X.*, et al.*, *Adv. Mater.* (2019) **31** (5).
114. Wang, H. X.*, et al.*, *ACS Appl. Mater. Interfaces* (2015) **7** (41), 22874.
115. Fei, W. W.*, et al.*, *Nanoscale* (2019) **11** (3), 1313.
116. Perez-Mitta, G.*, et al.*, *Adv. Mater.* (2017) **29** (28), 1700972.
117. Hou, X., *Adv. Mater.* (2016) **28** (33), 7049.
118. Zhang, Z.*, et al.*, *J. Am. Chem. Soc.* (2017) **139** (26), 8905.
119. Zhou, Y., and Jiang, L., *Joule* (2020) **4** (11), 2244.
120. Zhang, Z.*, et al.*, *Nat. Commun.* (2020) **11** (1).
121. Zhu, X. B.*, et al.*, *ACS Nano* (2017) **11** (11), 10816.
122. Zhang, X.*, et al.*, *Eng. Sci.* (2019) 7 (65). DOI: 10.30919/es8d505.
123. Yuan, B.*, et al.*, *ES Food Agrofor.* (2020) 1. DOI:10.30919/esfaf0004.
124. Dashairya, L.*, et al.*, *Adv. Compos. Hybrid Mater.* (2019) **2** (1), 70.
125. Li, G.*, et al.*, *Adv. Compos. Hybrid Mater.* (2019) **2** (2), 254.
126. Yun, J.*, et al.*, *ACS Appl. Mater. Interfaces* (2017) **9** (19), 16694.
127. Cai, J.*, et al.*, *ES Mater. Manuf.* (2019) **6**. DOI: 10.30919/esmm5f611.
128. Wang, Y.*, et al.*, *Adv. Compos. Hybrid Mater.* (2020) **3** (4), 473.
129. Zhao, Y. Y.*, et al.*, *Adv. Funct. Mater.* (2017) **27** (27).
130. Wang, Z.*, et al.*, *Chem. Commun.* (2019) **55** (96), 14486.
131. Luo, J. Q., and Wan, Y. H., *J. Membr. Sci* (2013) **438**, 18.
132. Gao, J.*, et al.*, *J. Membr. Sci* (2014) **452**, 300.
133. Zhang, B.*, et al.*, *Desalination* (2015) **357**, 208.
134. Sun, S. P.*, et al.*, *J. Membr. Sci* (2012) **401**, 152.
135. Zhao, S. S.*, et al.*, *J. Membr. Sci* (2015) **492**, 620.
136. Wu, C. R.*, et al.*, *J. Membr. Sci* (2016) **517**, 64.
137. Chen, Y. L.*, et al.*, *J. Membr. Sci* (2017) **537**, 407.
138. Guo, C.*, et al.*, *Sep. Purif. Technol.* (2020) **230**, 115567.
139. Liu, S. H.*, et al.*, *J. Mater. Chem. A* (2017) **5** (44), 22988.
140. Gao, Z. F.*, et al.*, *J. Membr. Sci* (2019) **574**, 124.
141. Zhang, Y.*, et al.*, *Mater. Today* (2020) **36**, 40.
142. Gao, Z. F.*, et al.*, *J. Membr. Sci* (2018) **565**, 169.
143. Guo, J.*, et al.*, *J. Membr. Sci* (2021) **619**, 118791.
144. Yang, F.*, et al.*, *Chem. Eng. Sci.* (2020) **225,** 115845.
145. Zhang, Y. Q.*, et al.*, *Sci. Adv.* (2021) **7** (13).
146. Wang, J. T.*, et al.*, *Adv. Funct. Mater.* (2019) **29** (23), 1900819.
147. Liu, J. T.*, et al.*, *Adv. Mater.* (2018) **30** (11), 1705933.
148. Li, C. X.*, et al.*, *ACS Appl. Mater. Interfaces* (2019) **11** (20), 18456.
149. Zhang, J. H.*, et al.*, *J. Membr. Sci* (2010) **349**, 295.
150. Yang, H.-C.*, et al.*, *J. Membr. Sci* (2017) **523**, 1.
151. Alkhudhiri, A.*, et al.*, *Desalination* (2012) **287**, 2.
152. Huang, Y. X.*, et al.*, *Environ. Sci. Technol.* (2017) **51** (22), 13304.
153. Li, M.*, et al.*, *J. Membr. Sci* (2020) **603**, 118031.
154. Chen, Y.*, et al.*, *Environ. Sci. Technol.* (2020) **54** (19), 12713.
155. Yang, Y. B.*, et al.*, *ACS Energy Lett.* (2018) **3** (5), 1165.
156. Xu, W. C.*, et al.*, *Adv. Energy Mater.* (2018) **8** (14), 1702884.

157. Xiao, P., *et al.*, *Nano Energy* (2020) **68**, 104385.
158. Zhao, Y. M., *et al.*, *Nat. Commun.* (2020) **11** (1).
159. Sheng, X., *et al.*, *J. Am. Chem. Soc.* (2017) **139** (36), 12402.
160. Wang, R. C., *et al.*, *Matter* (2019) **1** (5), 1274.
161. Moeini, A., *et al.*, *Carbohydr. Polym.* (2020) **233**, 115839.
162. Zhu, T., *et al.*, *Adv. Healthc. Mater.* (2018) **7** (7), e1701086.
163. Shen, Y. Z., *et al.*, *Chem. Eng. J.* (2021) **413**, 127455.
164. Liu, J., *et al.*, *Chem. Eng. J.* (2021) **408**, 127262..
165. Wan, X., *et al.*, *NPG Asia Mater.* (2019) **11** (1)
166. Arora, P., and Zhang, Z. M., *Chem. Rev.* (2004) **104** (10), 4419
167. Lan, Y., *et al.*, *Adv. Sci.* (2021), 2004036.
168. Liu, K., *et al.*, *Adv. Mater.* (2017) **29** (4), 1603987.
169. Oh, Y.-S., *et al.*, *Adv. Funct. Mater.* (2016) **26** (39), 7074.
170. Yang, H. C., *et al.*, *Adv. Mater. Interfaces* (2016) **3** (9), 1500774.
171. Pei, C. T., *et al.*, *ACS Nano* (2018) **12** (6), 5489.

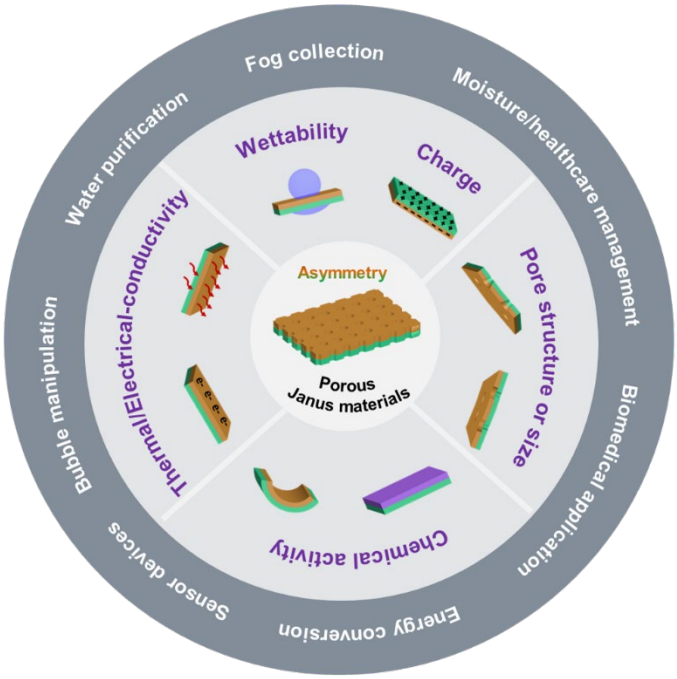

Fig. 1 Summary of the properties, functions, and potential applications of porous Janus materials based on various asymmetries (e.g. wettability, charge, pore size or structure, thermal or electrical conductivity, or chemical activity).

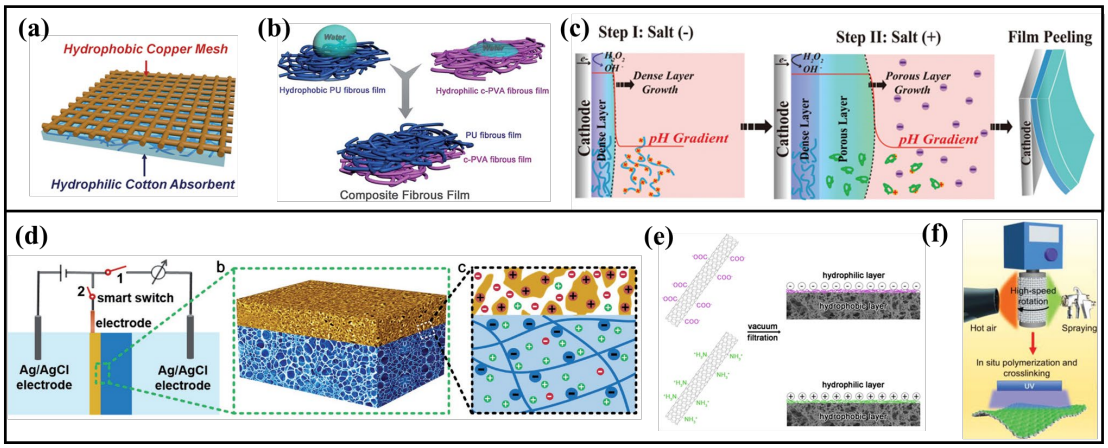

Fig. 2 Direct/sequential assembly into Janus materials. (a) Assembly of copper mesh and cotton absorbent [16]. Reproduced with permission, Copyright©2015 WILEY-VCH. (b) Bouble-layer fabrication by electrospinning sequentially [54]. Reproduced with permission. Copyright ©The Royal Society of Chemistry 2012. (c) Two-step electrodeposition [56]. Reproduced with permission, Copyright 2019 WILEY-VCH. (d) Chemical crosslinking followed by electrodeposition [53]. Reproduced with permission. Copyright © 2017 WILEY-VCH. (e) Deposition of CNT on the substrate by vacuum filtration [34]. Reproduced with permission. Copyright © 2018 American Chemical Society. (f) Spray-coating followed by in situ polymerization and crosslinking [32]. Reproduced with permission. Copyright© 2019 WILEY-VCH.

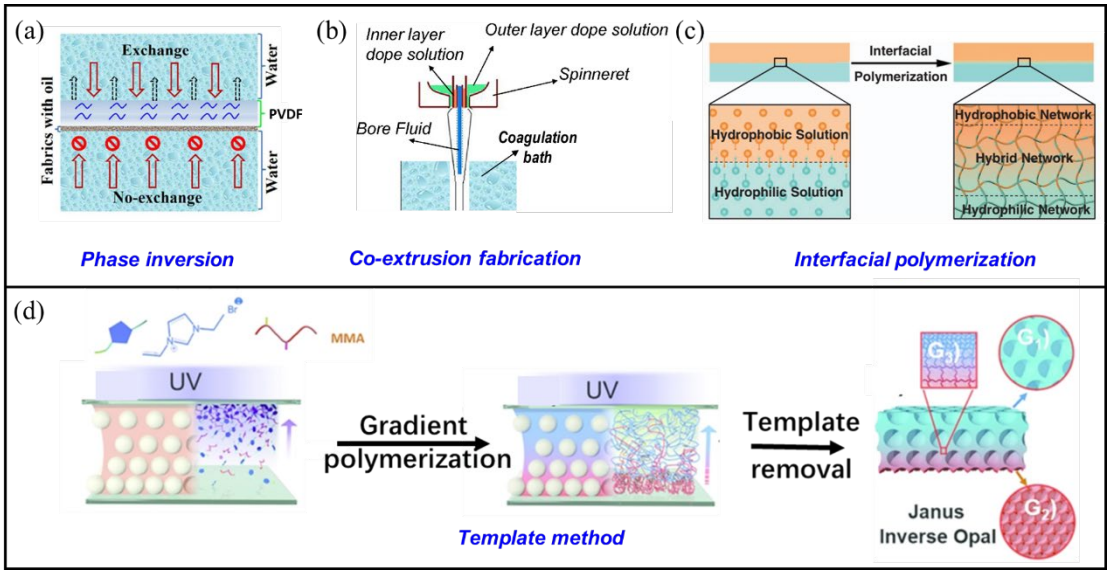

Fig. 3 In situ generation of Janus materials. (a) Phase inversion [66]. Reproduced with permission. Copyright© 2018 American Chemical Society. (b) Co-extrusion [67]. Reproduced with permission. Copyright© 2007 Elsevier B.V. (c) Interfacial polymerization [68]. Reproduced with permission. Copyright©2017, Springer Nature. (d) Photo-polymerization followed template removal [35] Reproduced with permission.Copyright © 2018 American Chemical Society.

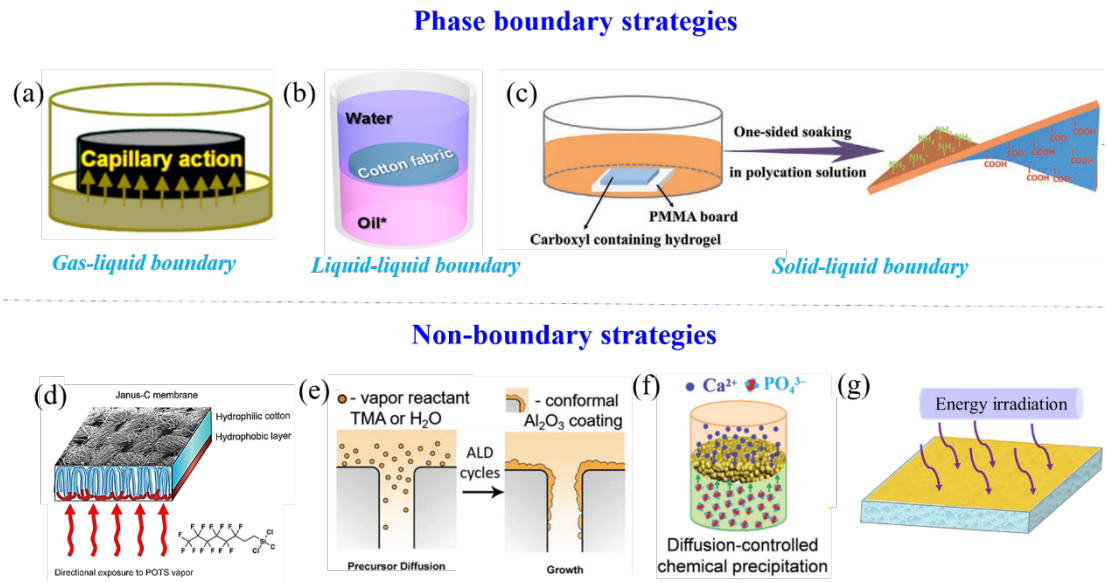

Fig. 4 The strategies of asymmetric modification into Janus materials. (a) Aerogel floating on the solution to introduce the gas-liquid boundary [70]. Reproduced with permission. Copyright © 2019 American Chemical Society. (b) The cotton fabric remaining at the oil/water interface for asymmetric modification [77]. Reproduced with permission. Copyright © 2019 Elsevier B.V. (c) PMMA board and the solution constructing the solid-liquid boundary for the hydrogel one-side modification [76]. Reproduced with permission. Copyright © 2020 Wiley-VCH GmbH. (d) Vapor diffusion [78]. Reproduced with permission. Copyright © 2014 WILEY-VCH. (e) Atomic layer deposition (ALD) [79]. Reproduced with permission. Copyright ©2018 WILEY-VCH. (f) Ion diffusion [83]. Reproduced with permission. Copyright © The Royal Society of Chemistry 2017. (g) Unilateral energy irradiation.

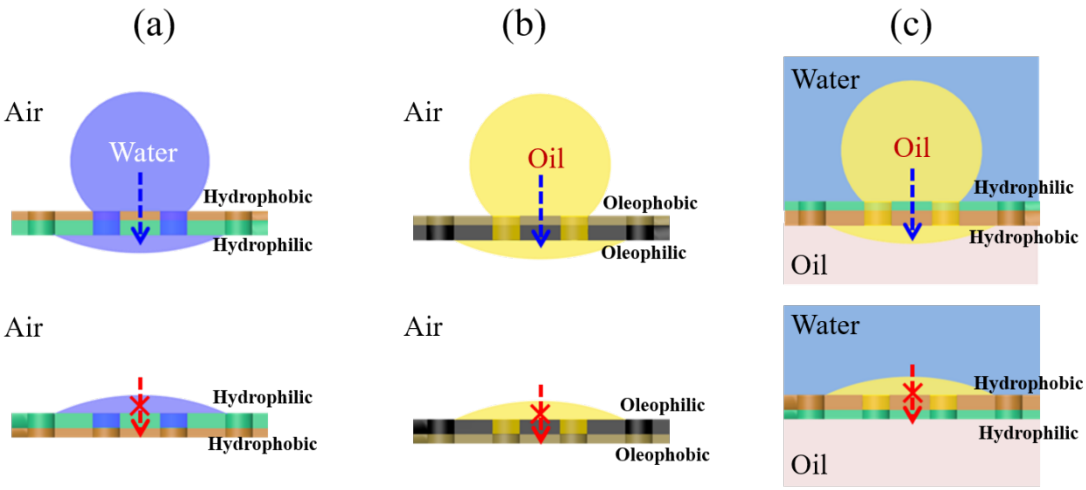

Fig. 5 Schematic diagram of directional liquid transportation. (a) Directional water transport in air. (b) Directional oil transport in air. (c) Directional oil transport under water.

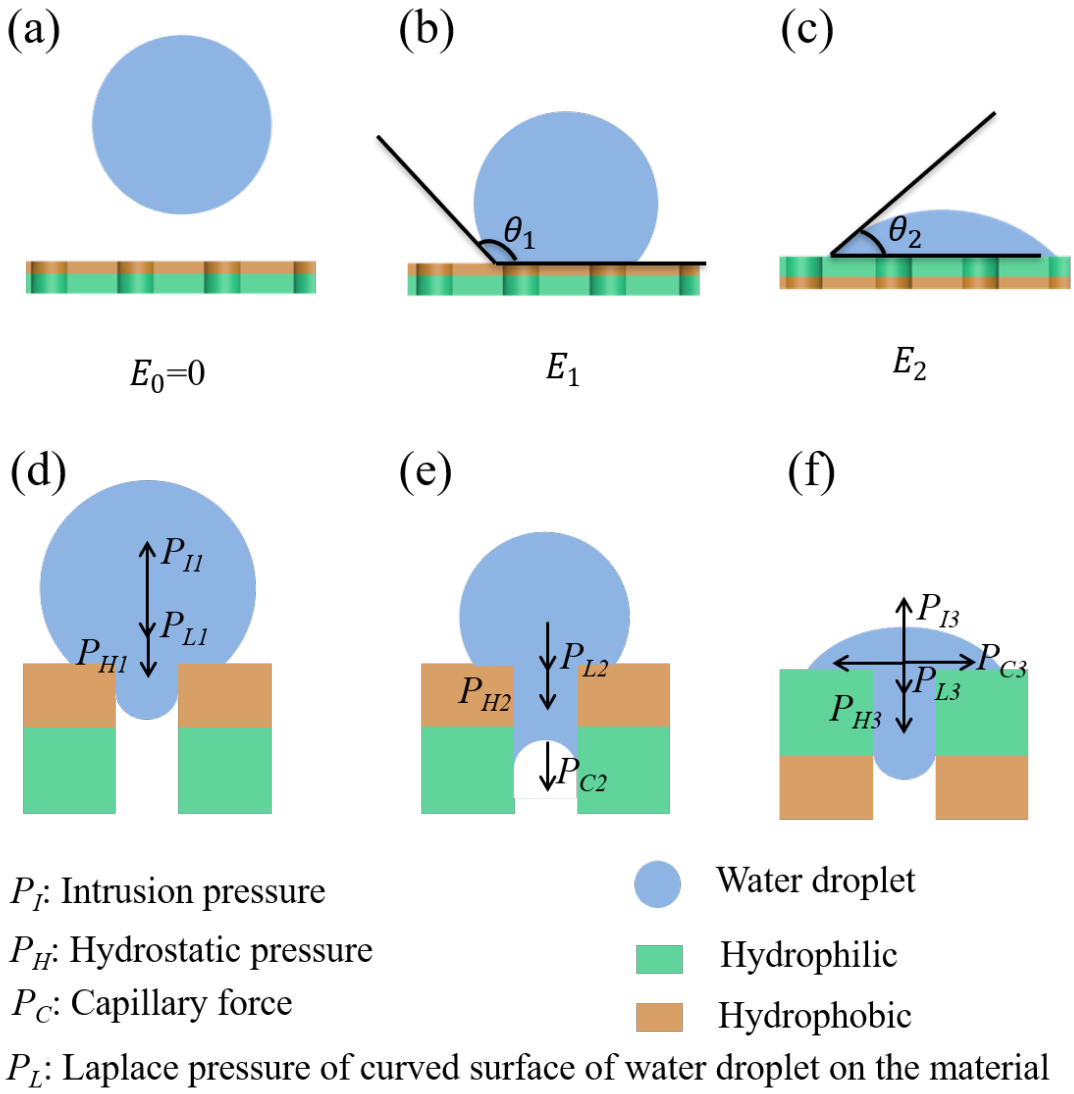

Fig. 6 The surface energy analysis of water droplets in original state (a), on the hydrophobic layer (b) and hydrophilic layer (c) of Janus materials. The force analysis of droplets on the hydrophobic layer (d and e) and the hydrophilic layer (f).

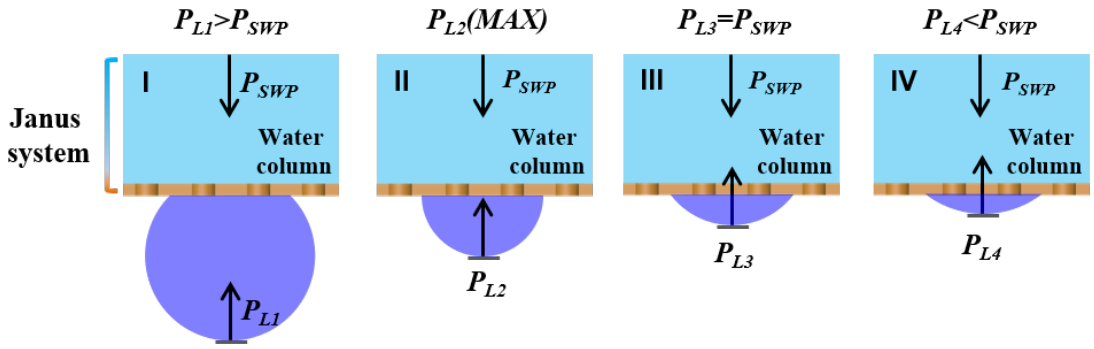

Fig. 7 The mechanism of the upper thin water column/superhydrophobic mesh Janus system for directional water transport.

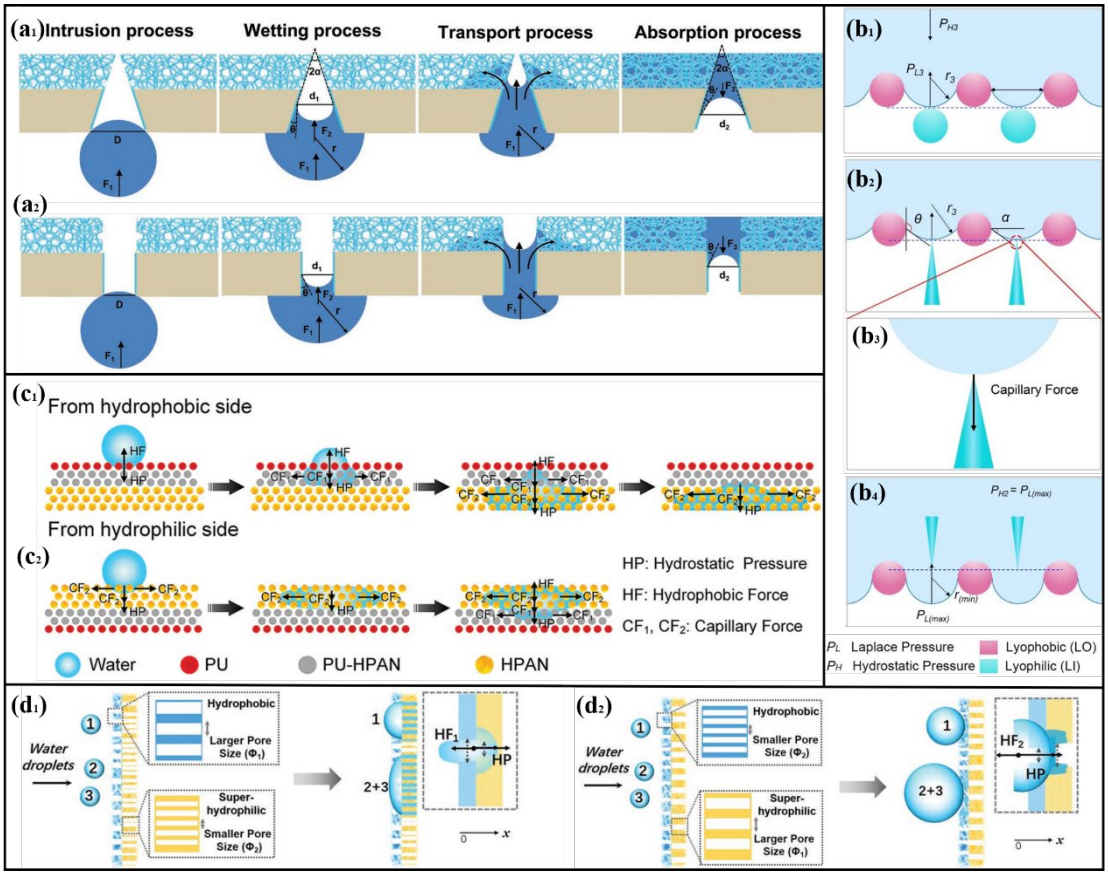

Fig. 8 ($a_{1\text{-}2}$) The mechanism of conical micropore enhancement [18] Reproduced with permission. Copyright 2019 WILEY-VCH. ($b_{1\text{-}4}$) The mechanism of nanoneedle enhancement [104]. Reproduced with permission. Copyright 2019 American Chemical Society. ($c_{1\text{-}2}$) The mechanism of tri-layered fibrous membranes enhancement [105]. Reproduced with permission. Copyright 2018 WILEY-VCH. ($d_{1\text{-}2}$) The mechanism of asymmetric pore size enhancement [55]. Reproduced with permission. Copyright 2019 WILEY-VCH.

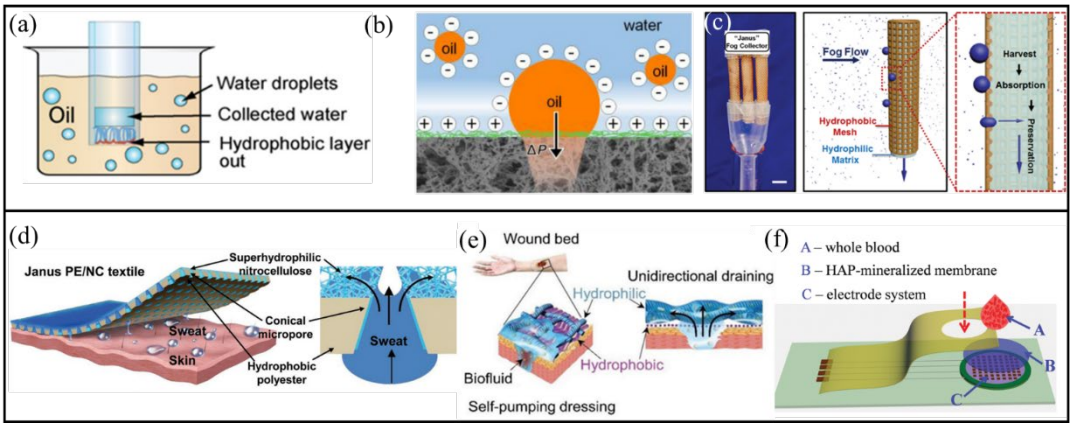

Fig. 9 (a) Water collection from oil phase by a Janus fabric equipped device [78]. Reproduced with permission. Copyright © 2014 WILEY-VCH. (b) Separation of oil-in-water emulsions by demulsification [34]. Reproduced with permission. Copyright © 2018 American Chemical Society. (c) A continuous Janus fog collector [16]. Reproduced with permission. Copyright © 2015 WILEY-VCH. (d) The sweat output from human body using the Janus PE/NC textile [18] Reproduced with permission. Copyright © 2019 WILEY-VCH. (e) The self-pumping dressing to accelerate wound healing by draining excessive biofluid [113] Reproduced with permission. Copyright © 2018 WILEY-VCH. (f) Porous Janus HAP-mineralized membrane for plasma separation and measurements of the glucose levels [83]. Reproduced with permission. Copyright © The Royal Society of Chemistry 2017.

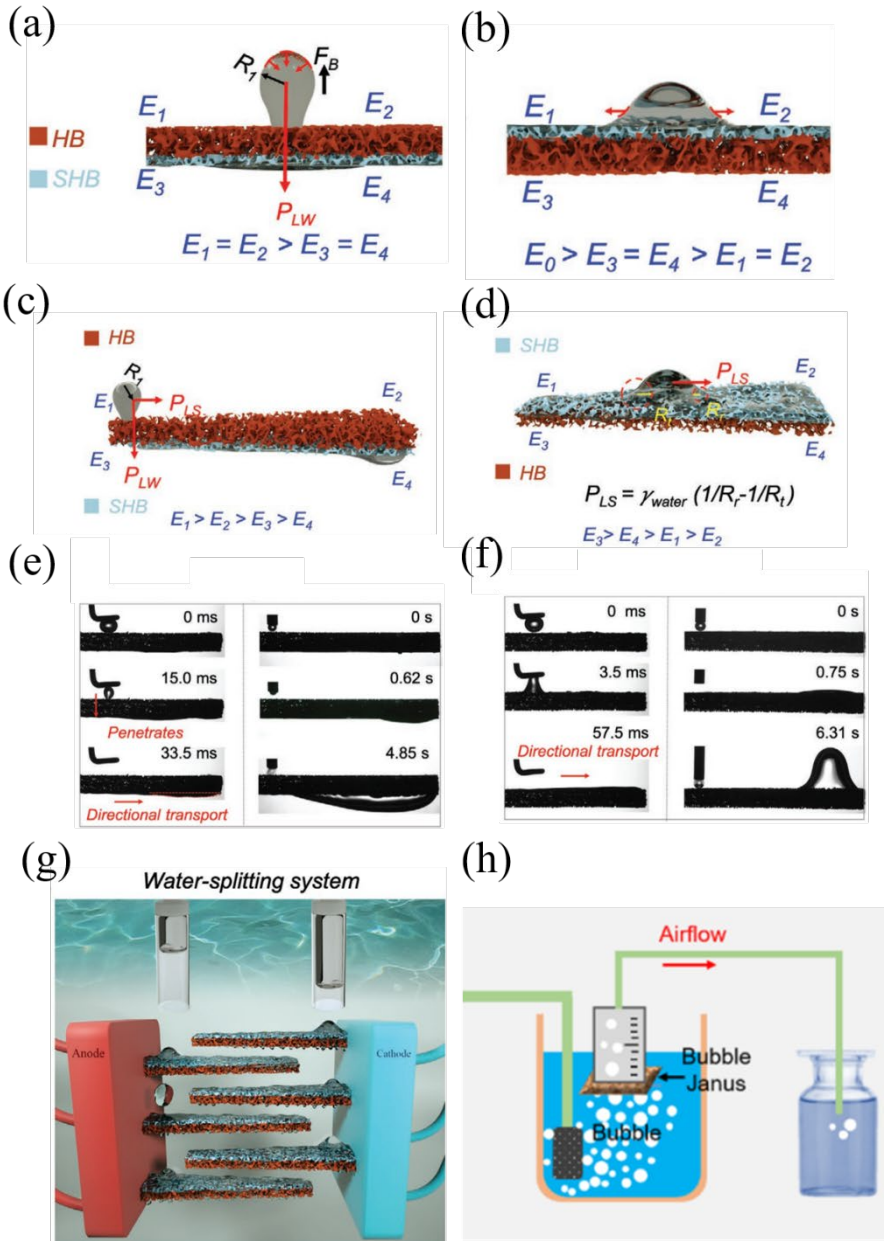

Fig. 10 Schematic of the mechanism of directional bubble transport under water with (a) aerophobic side upwards and (b) superaerophilic side upwards. (c) Schematic of the mechanism of bubble manipulation on the aerophobic side of the Janus foam and (e) corresponding time-lapse images. (d) The schematic of the mechanism of bubble manipulation on the superaerophilic side of the Janus foam and (f) corresponding time-lapse images. (g) The schematic of Janus electrode for water splitting [21]. (a-g) Reproduced with permission. Copyright © 2020 WILEY-VCH. (h) The schematic of Janus foam for CO_2 capture [20]. Reproduced with permission. Copyright © 2020 American Chemical Society.

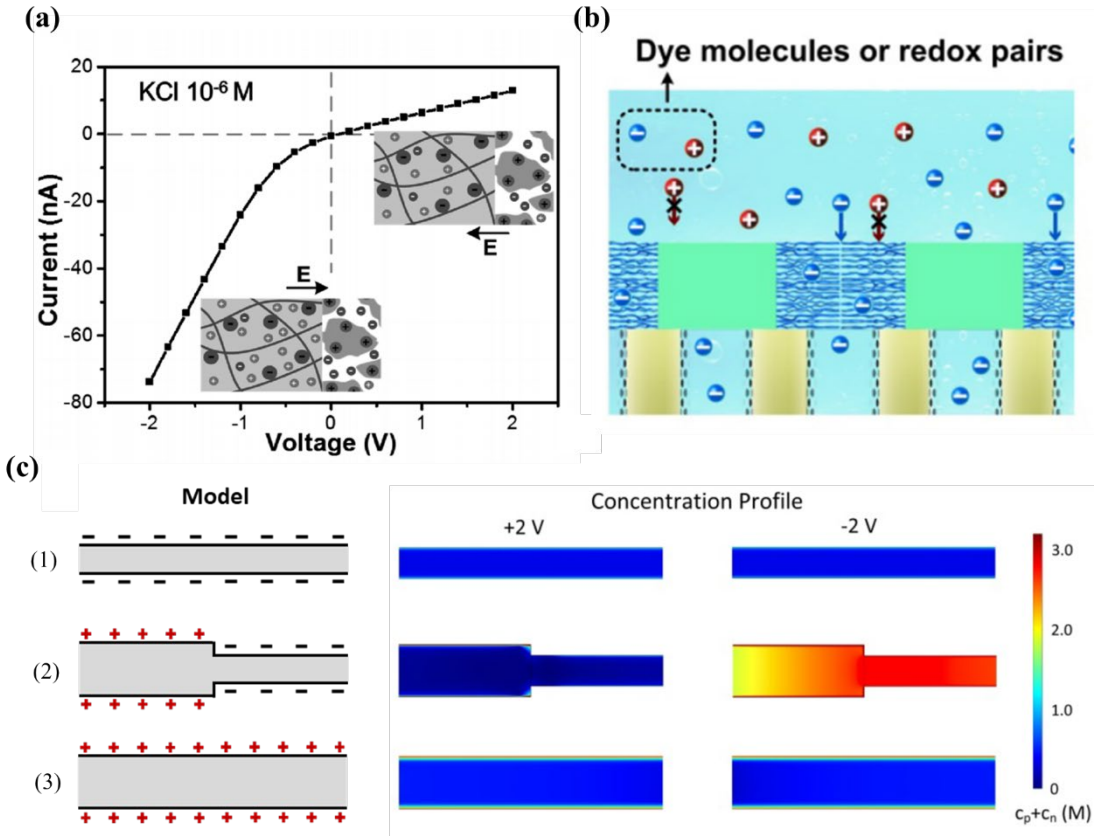

Fig. 11 (a) A typical I–V curve of the P(AAm-co-AA)/PPy heterogeneous membranes recorded in 1×10^{-6} M KCl solution. Inset shows the schematic illustrations of ion distributions at the interface in electrical fields with different directions [57] Reproduced with permission. Copyright © 2017 WILEY-VCH. (b) Excellent anion selectivity of the Janus membrane and (c) calculated ionic concentration distribution in positively charged, negatively charged, and Janus membranes [118]. Reproduced with permission. Copyright © 2017 American Chemical Society.

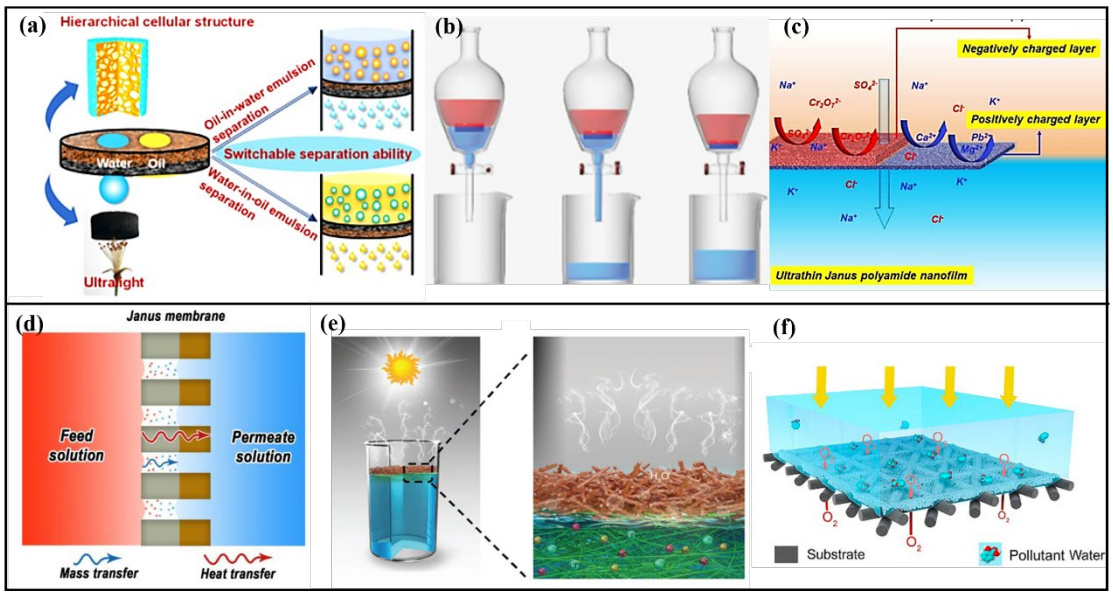

Fig. 12 (a) Switchable oil/water separation by a Janus aerogel [70] Reproduced with permission. Copyright © 2019 American Chemical Society. (b) The Janus gating for oil/water separation. [130] Reproduced with permission. Copyright © The Royal Society of Chemistry 2019. (c) Water-ions separation process of the Janus PA nanofilm with opposite charges [139] Reproduced with permission. Copyright © 2017 The Royal Society of Chemistry. (d) Membrane distillation process [150]. Reproduced with permission. Copyright © 2016 Elsevier B.V. (e) Solar steam generation and desalination [156] Reproduced with permission. Copyright © 2018 WILEY-VCH. (f) Enhancing photocatalytic reaction [159] Reproduced with permission. Copyright © 2017 American Chemical Society.

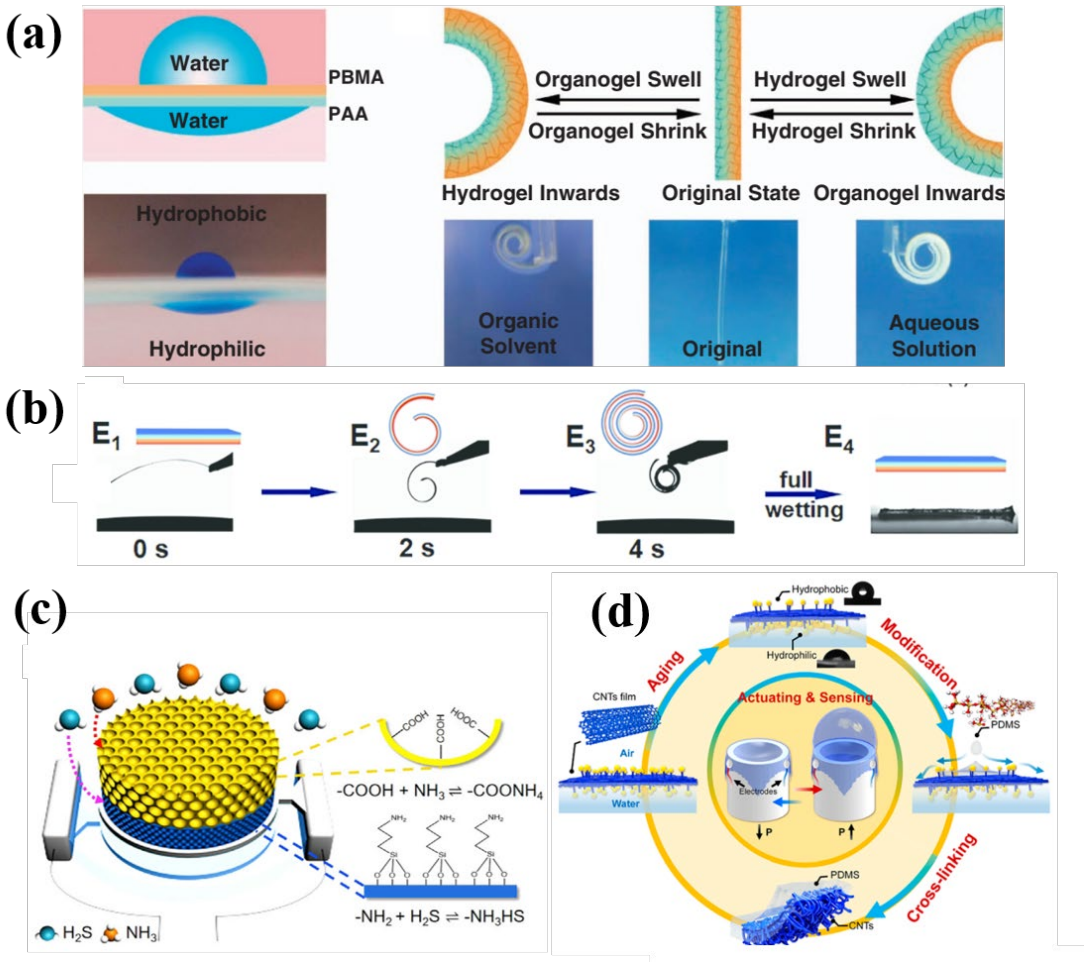

Fig. 13 (a) The wettability of the both sides of the hydrogel/organogel Janus film and the solvent response behaviour [68]. Reproduced with permission. Copyright © 2017, Springer Nature. (b) Actuator with vapor-response performance [35]. Reproduced with permission. Copyright © 2018 American Chemical Society. (c) Gas sensor devices [169] Reproduced with permission. Copyright © 2019 Elsevier Inc. (d) Janus film for noncontact sensing [58]. Reproduced with permission. Copyright © 2019 American Chemical Society.

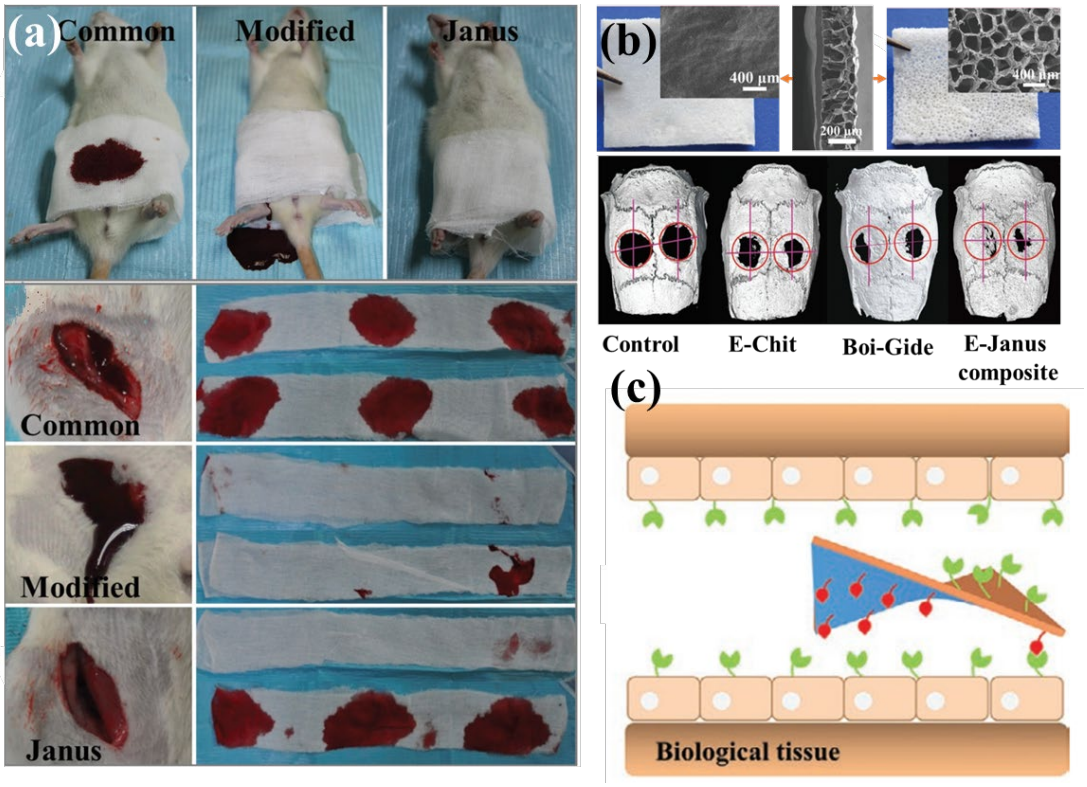

Fig. 14 (a) Contrast photos of double layer ordinary gauze, Janus gauze and hydrophobic modified gauze wrapped in injured rats. [162] Reproduced with permission. Copyright © 2018 WILEY-VCH (b) Guiding bone regeneration [56] Reproduced with permission. Copyright © 2019 WILEY-VCH. (c) Janus adhesives for internal tissue/organ repair and post-operative anti-adhesion [76] Reproduced with permission. Copyright © 2020 WILEY-VCH.

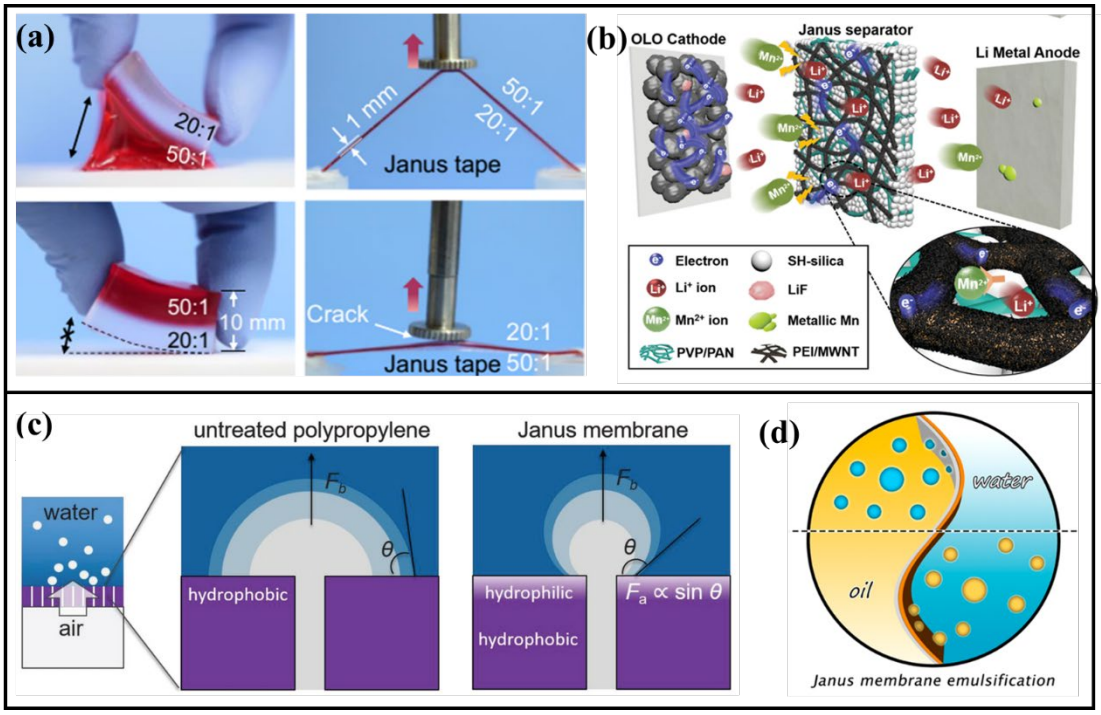

Fig. 15 (a) Janus PDMS tape shows apparent asymmetric adhesion performance of its two sides and can withstand large deformation [165]. Reproduced with permission. Copyright © 2019, The Author(s). (b) Battery separators [169]. Reproduced with permission. Copyright © 2016 WILEY-VCH. (c) Aeration [79]. Reproduced with permission. Copyright © 2018 WILEY-VCH. (d) The production of oil-in -water emulsion and water-in-oil emulsion [27]. Reproduced with permission. Copyright ©2017 American Chemical Society.